The Thesis Committee for May Mohammad El-Khattab Certifies that this is the approved version of the following thesis:

Post-permeation Stability of Modified Bentonite Suspensions under Increasing Hydraulic Gradients

APPROVED BY

SUPERVISING COMMITTEE:

_____

Chadi S. El Mohtar, Supervisor

_____

Robert B. Gilbert

Post-permeation Stability of Modified Bentonite Suspensions under Increasing Hydraulic Gradients

by

May Mohammad El-Khattab, B.E.

Thesis

Presented to the Faculty of the Graduate School of

The University of Texas at Austin

in Partial Fulfillment of the Requirements for the Degree of

Master of Science in Engineering

The University of Texas at Austin

August 2013

Dedication

To my loving parents, Mohammad and Fayrouz

and

To my guardian angel, my brother Mahmoud

Acknowledgements

I would like to thank my advisor, Professor Chadi El Mohtar, for his continuous support and treasured guidance both academically and non-academically. I would also like to thank Professor Robert B. Gilbert for his valuable feedback on my thesis.

I would like to express my perpetual appreciation to my classmate, Dr. Jisuk Yoon, for his guidance, support, and great achievements throughout this research. I would also like to thank Ritika Sangroya for her effort and help in conducting my experimental work, as well as, all my classmates at the University of Texas at Austin for providing insight into my research.

I would like to convey my gratitude to ExxonMobil for funding my research and my degree of Master of Science in Engineering at the department of Geotechnical Engineering at the University of Texas at Austin.

I would like to thank my parents, Mohammad and Fayrouz, and my dear brother Mahmoud for supporting me while I was pursuing my Master's degree.

Post-permeation Stability of Modified Bentonite Suspensions under Increasing Hydraulic Gradients

May Mohammad El-Khattab, M.S.E.

University of Texas at Austin, 2013

Supervisor: Chadi El Mohtar

ABSTRACT

Slurry wall is a geotechnical engineering application to control the migration of contaminants by retarding groundwater flow. Sand-bentonite slurry walls are commonly used as levees and containment liners. The performance of bentonite slurry in sand-bentonite slurry walls was investigated by studying the rheological properties of bentonite suspensions, the penetration length of bentonite slurry into clean sand, and stability of the trench under in-situ hydraulic gradients.

In this study, the rheological parameters of bentonite suspensions were measured at various bentonite fractions by weight from 6 to 12% with 0-3% of sodium pyrophosphate; an ionic additive to control the rheological properties of the bentonite slurries. The penetrability of the bentonite slurries through Ottawa sand was studied by injecting the slurries into sand columns at different bentonite fractions. The injection tests were performed with the

permeameters having different diameters to eliminate any bias on test results due to the different size of permeameter. An empirical correlation for predicting the penetration length of bentonite slurry based on apparent viscosity, yield stress, effective particle size, relative density, and injection pressures was updated by taking into account the effects of the permeameter diameter size.

Moreover, the stability of sand-bentonite slurry walls was inspected by studying the hydraulic performance of sand permeated with bentonite suspensions under increasing hydraulic gradients. The critical hydraulic gradient at which washing out of bentonite suspensions is initiated was examined. For specimens with bentonite contents less than the threshold value, the flow occurred through the sand voids and minimal washing out occurred. On the other hand, when the bentonite content was high enough to fill up all the void space between the sand particles, the flow was controlled by the clay void ratio. In this case, washing out did occur with increasing gradients accompanied by an increase in hydraulic conductivity. Accordingly, a relation between the yield stress of bentonite suspensions and the critical hydraulic conductivity was developed.

LIST OF CONTENTS

LIST OF TABLES

LIST OF FIGURES

LIST OF EQUATIONS

CHAPTER 1: INTRODUCTION

1.1 Problem Statement

Soil-bentonite mixtures are commonly used in levee construction to create a hydraulic barrier and retard water flow. Also, these mixtures are efficient in waste water and waste confinement. However, disastrous consequences tend to occur when the soil-bentonite barriers fail. For the past century, levee failures and subsequent floods have caused life loss and massive property damages in the United States. During Hurricane Katrina in 2005, three major levee breaches inundated the city of New Orleans, Louisiana. Thousands of lives were lost and damages worth over a 100 billion were generated. Most recently, a levee failure in Moonachie, NJ during hurricane Sandy caused over a thousand people to evacuate the town which was flooded with a water level up to 1.5 meters.

There are different mechanisms by which levees fail and one of them is under seepage. Under seepage occurs when the level of water increases on one side of the river causing the water flow through the underneath granular material to increase. This creates sand boils and open channels at the toe of the level which eventually lead to the levee failure. Under seepage problems are mitigated by permeating the granular material with bentonite to create soil-bentonite mixtures. However, it is important to understand the behavior of these soil-bentonite mixtures by understanding the rheological properties of bentonite suspensions and the mechanism of permeating sand with bentonite. Moreover, the stability of the soil-bentonite mixtures is essential to avoid levee failure. And so, the stability of the bentonite suspensions in the permeated soil under increasing hydraulic gradients should be investigated. Once the critical

hydraulic gradients is exceeded, bentonite suspensions will washout increasing the hydraulic conductivity of the soil-bentonite mixture and ultimately leading to the failure of the levee.

1.2 Research Objectives

The objective of this research is to evaluate the performance of Sand permeated with bentonite suspensions under various hydraulic gradients to ensure the stability of these mixtures against ground water flow. The effect of the rheological properties of bentonite suspensions on the hydraulic conductivity and stability of the Sand permeated with bentonite suspensions was investigated. The rheological properties were examined over time and controlled by altering the concentration of bentonite suspensions and an ionic additive (sodium pyrophosphate). Yoon; (2011) developed an empirical equation that estimates the penetration depth of bentonite suspensions into sand based on the properties of the sand and bentonite. The equation was adjusted in this study to accommodate for effects of permeameter diameter on the penetration depth. However, the main purpose of this research is to investigate the rheological properties of bentonite suspensions that govern the stability of the Sand permeated with bentonite suspensions under high hydraulic gradients. Specifically, the investigation focued on developing a relation between the yield stress of bentonite suspensions and the critical hydraulic gradient at which washing out occurs. The relation will help in estimating the minimum required bentonite suspension yield stress to ensure the stability of the suspension within the porous medium.

1.3 Organization of Thesis

The thesis structure includes six main chapters. Chapter 1 is an introduction to the thesis that includes the problem statement, research objectives, and thesis organization. Chapter 2 presents a detailed literature review on rheology, permeation, hydraulic conductivity, and

stresses in permeated soils. The distribution of stresses and strains of fluids in porous media is discussed in depth.

Chapter 3 describes in details the experimental program adopted for this study. The program includes materials, equipment, and setups used for the rheology, permeation, and washing out tests. The physical and chemical properties of the sand, bentonite, filter material, and water used are characterized in this section. The sample preparation process for both the permeation and washing out setups are included. Moreover, the rheometer, pressure panel, differential pressure transducers and their calibration are defined.

The rheological properties of bentonite and the results of the permeation and washing out tests are discussed in Chapter 4. The rheological properties are linked to the permeation results to estimate the penetration depth of bentonite into sand. The properties are also related to the washing out results to predict the failure of Sand permeated with bentonite suspensions. Chapter 5 includes a full analysis of the results. The equation to estimate the penetration depth is introduced, as well as, the relation to estimate the hydraulic gradient at which washing out of bentonite occurs.

The last chapter of the thesis, Chapter 6, summarizes the conclusions derived in this study. The conclusions were made regarding bentonite suspension permeation into sand and their washing out when subjected to high hydraulic gradients. This chapter also includes recommendation for future research.

CHAPTER 2: LITERATURE REVIEW

2.1 Introduction

The mechanism and case histories of under seepage are discussed in the literature review to fully understand the objective of this study which is evaluating the performance and stability of cut-off walls. Multiple types of cutoff walls are identified and soil-bentonite walls are explained further. Moreover, a thorough review of the literature on bentonite, rheology, permeation, hydraulic conductivity, and stability of sand-bentonite walls is presented to outline the scope of the study.

2.2 Under seepage

Earth and rock-fill dams are subject to seepage through the embankment, foundation, and abutments; whereas, levees are at risk of failure due to under seepage. Seepage occurs due to differential hydrostatic pressures which are easily transferred through permeable sand layers underneath the top soil. If the hydraulic head is large enough, the water flow may mobilize sand grains causing erosion and ultimately instability and failure of the levee or dam. Therefore, seepage control is necessary to prevent excessive uplift pressures, instability of the downstream slope, piping through the embankment and foundation, and erosion of material.

2.2.1 Mechanism of under seepage

Under seepage, also known as seepage, occurs from the top stratum on the riverside towards the landward. A high hydraulic difference initiates the flow through the granular deposits under the dam or levee. Once the water pressure exceeds the submerged unit weight of the top soil on the landside, heaving and/or piping occurs. Figure *2-1* shows the different forms of seepage leading to levee failure. Heaving and piping are the most dominant failure

mechanisms of under seepage. Heaving happens when the under seepage forces push the substrata upwards, while piping is the process of retrograde erosion in the sandy layers underneath levees. When the vertical seepage forces, caused by the upward flow on the landslide, surpass the weight of the top soil, the water flow carries and deposits sand grains at the surface creating sand boils. Sand boils are usually created when a critical gradient of 0.85 for silty sands and sand, and 0.8 for silty clay and clay is exceeded (Turnbull and Mansur, 1959).

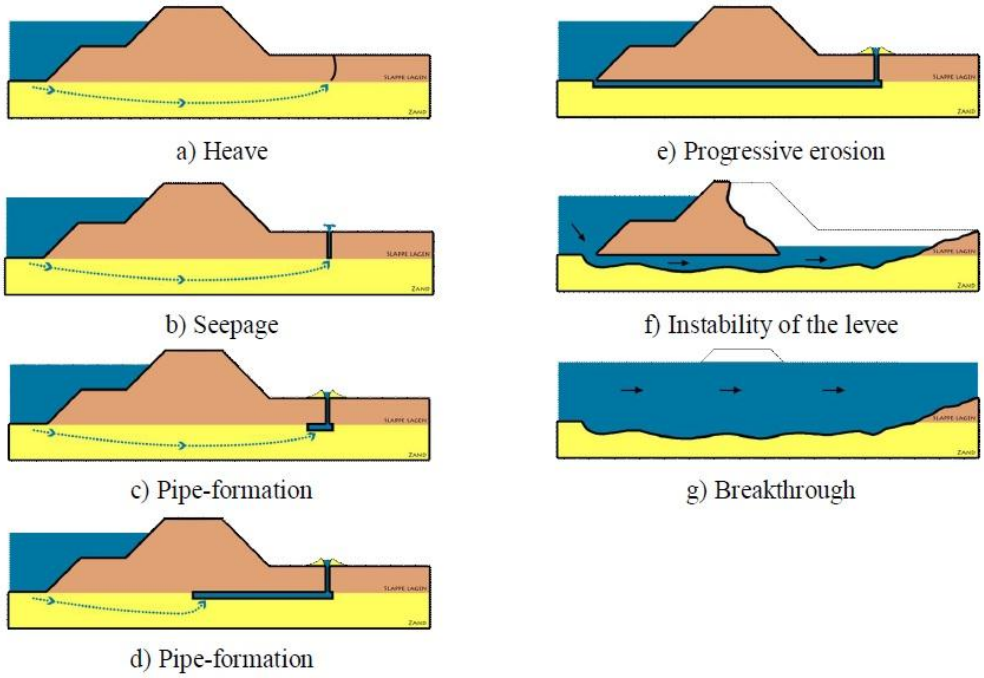

Figure 2-1: Under seepage mechanism (Adopted from Vries, Koelewjin, and Hopman)

2.2.2 Case histories of levee failure

Over the past century, many levee failures occurred due to seepage causing little or massive destruction to the surrounding area. This section focuses on three major level failures that are considered to be massive because of the lives lost and/or great destruction incurred.

Great Flood of 1993

The size and impact of the Great Flood of 1993 was unprecedented and has been considered among the most costly and devastating flood to occur the United States. Damages were estimated to $15 billion and 38 lives were lost. The flood affected an area of 30,000 square miles. It was named the "Great Flood" because of the number of record river levels, aerial extent, number of persons displaced, amount of crop and property damage and its duration which exceeded all earlier floods in the U.S.A.

The Great Flood of 1993 occurred in the Illinois area near the Upper Mississippi River basins in May-August 1993. Uniquely extreme weather and hydrologic conditions led to the flood of 1993. After the heavy rain in 1992, July brought heavy rain to the Missouri and upper Mississippi River basins in Missouri, Iowa, Kansas, Nebraska, North and South Dakota, Illinois and Minnesota. Precipitation for the month averaged from one inch above normal at St. Louis and Springfield, to between six and seven inches above normal at Columbia and Kansas City, Missouri. The 1993 flood broke the record river levels set during the 1973 Mississippi and the 1951 Missouri River floods.

On August 1, a levee broke near Columbia, Illinois which flooded 47,000 acres of land, inundating the towns of Valmeyer and Fults, Illinois. The released water continued to flow parallel to the river approaching the levees protecting historic Prairie du Rocher and Fort de Chartres, Illinois. On August 3, a decision has been made by the Corops of Engineering to break down a portion of the stronger Mississippi River levee to release the water back into the river.

Nearly all of the 700 privately built Missouri river agricultural levees were overtopped or destroyed. Levees along the Mississippi river failed due to excessive under seepage and internal erosion. A large sand boil of 600 to 1500 feet formed along the river. The top layer consisted of alluvium layers with thickness of 10 to 25 feet; whereas, the bottom layer consisted of highly pervious sands with thickness ranging from 100 to 150 feet and hydraulic conductivity ranging from $3.5x10^{-2}$ cm/sec to $1.2x10^{-1}$ cm/sec (Turnbull and Mansur, 1959).

Sacramento San Joaquin River Delta

The Sacramento- San Joaquin River Delta, also known as California Delta, is an expansive inland river delta in North California in the United States. The 1,100 km of waterways in the delta are surrounded by 1,800 km of levees. A typical trapezoidal levee was constructed to be 10 feet above the original ground level. The levee allowed 2,000 km^2 of land to be used for agricultural purposes. The delta which is below sea level provides freshwater to central and southern California; therefore, it is crucial to keep it clear from saltwater.

There have been over 160 levee failures in the Sacramento-San Joaquin River since 1900. The failures were caused by water overtopping the levees or structural failure due to seepage and erosion. The most recent level failure happened in June 2004 and caused more than 190,000,000 m^3 of water to flood the island of Jones Tract. The foundation of the levees are composed of river sediments and organic materials including gravel, loose sand, silts, clays, and peat. The hydraulic conductivity of the sand layer was estimated to be 10^{-3} cm/sec.

Hurricane Katrina

Hurricane Katrina was one of the five deadliest and most destructive hurricanes in the history of the United States. It hit east of New Orleans on August 29, 2005 killing 1,833 people and causing $81 billion worth of damages. It was the costliest natural disaster. Multiple lessons especially on levee design were learned from hurricane Katrina. There were 50 major breaches in the Hurricane Protection System during the hurricane. The levees failed primarily as a results of system design flaws. The levees that were constructed using hydraulic fill and higher silt and sand were severely damaged; whereas, those constructed using cohesive materials survived.

At the London Avenue Canal, the levees and I-walls were made of a marsh layer overlying beach sand. The south breach of London Avenue was due to seepage and piping where identical beach sand was found in the neighborhood and on the protected side of levee. Seepage caused the levee to become unstable and ultimately failing completely. The north breach of the London Avenue failed due to sliding instability caused by high uplift pressures in the sand layer acting at the base of the clay layer. Although piping was present, heaving was the main reason for causing the levee to slide and fail.

2.2.3 Mitigation of under seepage

Under seepage can be controlled by constructing riverside blankets, relief wells, seepage berms, and cutoff walls. Riverside blankets reduce landward pressure and seepage by preventing water from leaking into the top thin layer of granular material. These blankets consist of impervious soils with a hydraulic conductivity ranging from 10^{-5} to 10^{-6} cm/s (Kolb, 1976). They should be protected from erosion by waves and runoff. A blanket is less efficient when constructed upstream when compared to landslide (Wolff, 1987).

Relief wells are made of pervious material that release uplift pressure beneath the levee. Relief wells are a convenient seepage mitigation method because they require low right-of-way for construction, and are very flexible so intermediate wells can be introduced to release more pressure. However, relief wells may be expensive to be constructed if high uplift is present. Extra measures must be taken to keep the well open during boring and installation of the screen and filter (Wolff, 1987). Also, the wells need to be periodically inspected to prevent clogging and back-flooding.

Seepage berms are another mitigation method because they provide additional weight to counter the upward forces and create a longer seepage flow path. The four types of berms: impervious berms, semi-pervious berms, sand berms, and free-draining berms, can be used and the selection is usually based on fill materials availability and cost. Berms are easy to construct, require low maintenance, and protect against sliding of the levee slope. However, they require large space and may be expensive depending on material availability. Seepage berms cannot be used for foundation seepage. Impervious berms with low hydraulic conductivity reduce seepage, but increase uplift pressure downstream. Pervious berms must be carefully designed to prevent foundation material from migrating upwards and clogging them (Wolff, 1987).

Cutoff walls are widely used to prevent seepage by lengthening the seepage path. The most common type of cutoff walls include sheet piles, deep soil mixing, and slurry walls. Sheet piles are steel sheets driven by a hammer to form a continuous wall. Such cutoff walls are strong, contains water and soil, resists chemical erosion, and does not require excavation. However, they cannot be installed in hard rock soil and are limited to a penetration depth of approximately 100 to 150 feet (Smyth et al., 1995). Also, leaks might occur at splices and torn interlocks. Deep soil mixing is the technique of constructing large masses of soil and additive mixture to create a

barrier. Additives include bentonite, cement, lime, fly ash, and slag. These walls can go to a depth of 100 feet and must be vertical.

Slurry walls are commonly used as subsurface barrier to lateral flow of groundwater and to water-borne pollutants. They are used to prevent migration of contamination through groundwater, prevent infiltration of surface water into the contaminated area, and prevent contact with contaminated materials. Soil-bentonite cutoff walls are constructed by excavating a continuous narrow trench while permeating with bentonite slurry to keep the excavation stabilized; no need for other lateral supports such as shoring. The trench is backfilled with a mixture of the excavated soil and bentonite displacing the bentonite slurry. Soil-bentonite cutoff walls are practical because they do not require wide access areas and are typically up to 200 feet deep (Pearlman, 1999). However, these walls require excavation, disposal of material, and space for mixing. Its limitations include the necessity of a vertical direction, the absence of a groundwater table and the need to go through all top soils down to the problematic zone, even if the top soils do not need the slurry wall. Soil-bentonite cutoff walls may fail due to cracking caused by shrinkage, thermal stress, and wet/dry cycling (Heiser and Dwyer, 1997). Figure 2-2 shows that installation process of soil-bentonite cutoff walls.

Figure 2-2: Installation process of soil-bentonite cutoff walls (Adopted from www.geo-solutions.com)

2.3 Bentonite

Bentonite is characterized with very unique and valuable properties that make it useful in a great number of different applications. Bentonite is used as a bonding material in preparing molding sand for the production of cast iron, steel, and non-ferrous casting. It is also used in agriculture for soil improvement, in water treatment for its ion exchange and flocculation, in ceramics to enhance paste plasticity, in paper to improve its quality, in wine making to enhance clarification and protein stabilization, in pharmaceuticals, cosmetics, and spa mud therapy.

However, mostly importantly, bentonite's rheological properties and thixotropy cause bentonite to be used as a constituent for oil and water well drilling to stabilize and seal borehole and remove drilling cuttings. Bentonite slurries are commonly employed in the construction of foundation for diaphragm walls and bored piles. Since bentonite is a self-hardening mixture and waterproof, it is used to build cut off walls, grouting mortars, grouting, seal soil infiltrations, and line the base of landfills.

2.3.1 Bentonite particles

Bentonite is a clay mainly constituted of the mineral montmorillonite; therefore, it has a high plasticity and swelling potential. Bentonite particles consist of an octahedral Alumina sheet sandwiched between two tetrahedral Silica sheets. The alumina sheet is composed of an aluminum, iron, or magnesium atom equidistant from six hydroxyls of oxygen or hydroxyls. The atoms are tightly packed in an octahedral structure. Similarly, the Silica sheet includes a silicon or aluminum atom equidistant from four oxygen atoms tightly packed. The octahedral and tetrahedral sheets are symmetric and share the oxygen atoms to form a unit layer. The units are stacked on top of each other in a parallel manner to form a Hoffman structure. The bonds in the unit are covalent and hence stable; however, the crystal lattice formed between the units is unstable. Van der Waals forces connect the units together, and so they are easily separated by the adsorption of water and other polar molecules (van Olphen, 1977). The surface of the layers is negatively charged due to isomorphic substitutions; cation replacement of Si^{4+} by Al^{3+} in octahedral layer, and replacement of Al^{3+} by Mg^{2+} in tetrahedral layer. Figure 2-3 shows the atomic structure of the montmorillonite.

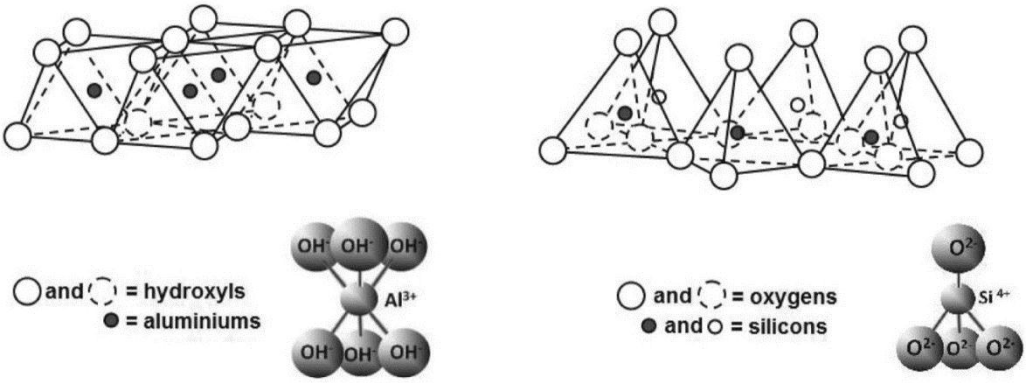

Figure 2-3: Atomic structure of Montmorillonite (Adopted from geoscienceworld.org)

2.3.2 Bentonite suspensions

A double diffuse layer is developed at the clay surface when in an aqueous medium because clay is negatively charged. Ions in the aqueous medium are located in between the unit layers in the stack and at the stack surface (van Olphen, 1977). An adsorbed layer of ions surrounds the particle surface and the concentration of ions decreases non-linearly as the distance from surface increases (Stern,1924). As for the charges at the edges, it is determined by the transportation of H^+ and OH^- in the aqueous medium. The isoelectric point is the pH at which the edges have a zero charge, it is known to be between 5 and 8 (Duran et al., 2000). At pH values greater than the isoelectric point, the edges are negatively charged; whereas, they are positively charged at pH values lower than the isoelectric point (van Olphen, 1977). The chemical reactions involved are as follows (Tombacz and Szekeres, 2004):

$$Al\text{-}OH\text{-}H^+ \leftrightarrow Al\text{-}OH_2^+$$

$$Al\text{-}OH\text{-}OH^- \leftrightarrow Al\text{-}O^-$$

$$Si\text{-}OH\text{-}OH^- \leftrightarrow Si\text{-}O^-$$

It is crucial to determine the stability of the clay particles in aqueous medium; therefore, the zeta potential is important. The zeta potential is the potential in the diffuse double layer between the fixed part and the mobile part. A high zeta potential implies that the colloids are stable; whereas, a low zeta potential implies high repulsion and flocculation. The zeta potential in sodium bentonite slurry is negative, almost insensitive to pH, and increases with increasing ionic strength (Callaghan and Ottweill, 1974). The stability of the clay particles is a function of the interparticle double layer repulsion energy and the Van der Waals attractive energy. Depending on the pH of the aqueous medium, the behavior of bentonite particles differs. The

repulsion forces decrease and the attraction forces increase when the concentration of cations in the aqueous solution increases. Contrarily, repulsion increases and attraction decreases with anions are abundant.

2.3.3 Orientation of bentonite particles

The orientation of the bentonite particles in aqueous medium depends on the particle charges and hence on the pH. In acidic environment where the pH is less than the isoelectric point, the particles edges and face are strongly attracted. This is due to the attraction between the negative face and the positive charges created at the particle edges due to hydrogen adsorption. Also, the face to face repulsion is increase due to the presence of dissolved ions (Lagaly, 1989). A 'card-house' structure is hence created in the bentonite suspensions (van Olphen, 1977). As the pH decreases and more H^+ are present in the solution, the edge to face attraction increases and the particles form a cluster which moves independently under applied stress. However, as the pH increases, the attraction bonds are weakened and unstable edge to edge contacts are formed (Lagaly, 1989).

In alkaline environment, the edges of the bentonite particles are negatively charged due to the adsorption of OH^-. In dilute solutions, the bentonite particles are diffused because they are repelled from each other. In more concentrated solutions, the repulsion is reduced; however, the particle rotational and transitional motion is restricted. This causes the particles to be in 'band-like' structure where the particles are placed in a parallel orientation (Fukushima, 1984). Nonetheless, if two particles approach each other, the Ca^{2+} ions create attractive electrostatic potential between the edges and between the edges and the face. This produces voluminous networks with greater yield stress and viscosity (Lagaly, 1989).

The concentration of bentonite and hence the concentration of Na^+ affects the orientation of the bentonite particles in aqueous solution, but it is dependent on pH conditions as well. In acidic medium, as the concentration of Na^+ increases, the stability of the card-house structure increases. However, if the medium becomes very acidic, face to face attractions are created decreasing the stability of the structure. In alkaline medium, the addition of Na^+ increases the stability of the band-like structure. Yet the addition of too much Na^+ weakens the structure.

2.3.4 Bentonite particles with ionic additives

The addition of ionic additives such as sodium hydroxide, sodium silicate, and poly-phosphate reduces the viscosity and yield stress of bentonite suspensions and therefore, increasing its mobility (Abend and Lagaly, 2000). The effect of ionic additives on bentonite suspensions varies depending on bentonite characteristics such as particle size, shape, surface charge, cation exchange capacity, and type of exchangeable cations (Goh et al., 2011). Sodium polyphosphate (SPP) decahydrate was used in this study because of its ability to effectively reduce yield stress and viscosity of bentonite suspensions. SPP modified suspensions produce a much lower yield stress right after mixing; however, it increases as the clay starts to flocculate and recovers a large portion of its strength after 24 hours of mixing.

The yield stress of bentonite suspensions decreases upon the addition of polyphosphates because of increased negative charges and repulsion between particles (Penner and Largaly, 2001). The increased negative charge is due to the attachment or adsorption of polyphosphate ions at the particles' edges by OH^- exchange. Although the phosphate ions disperse the bentonite suspensions, coagulation also occurs due to the presence of exchangeable cations and Brownian motion of particles. Critical coagulation concentration is achieved when the concentration of the additives is sufficient to initiate coagulation. The negatively charged faces are aligned in a

parallel orientation due to repulsion (Mourchid et al., 1995). This causes coagulation to occur due to attraction between the edges (Penner and Lagaly, 2001). The presence of SPP in bentonite suspensions increases the concentration of cations (Ca^{+} and Na^{+}) which in return increases coagulation. The abundant cations reduce the thickness of the diffuse layer which increase the attraction at the edges (Branderburg and Lagaly, 1988). Therefore, the bentonite network is built up faster and the bonds between particles is faster in modified suspensions compared to pure bentonite suspensions. The effect of additives is greater in diluted suspensions.

2.4 Rheology

The ability to permeate porous media with grout is highly dependent on the rheological properties of the grout; therefore, the theory behind rheology is introduced and discussed thoroughly in this section.

2.4.1 Theory of rheology

Rheology is the study of deformation and flow of matters based on Hooke's law of elasticity and Newton's law for viscous fluids. For relatively small stresses, stresses and strains are related linearly through a constant. Beyond this range, the material tends to exhibit strain softening or hardening behavior. Equations 1 and 2 show Hooke's law for elastic material.

$$\sigma = E\varepsilon \qquad \text{Equation 1}$$

$$\tau = G\gamma \qquad \text{Equation 2}$$

Where σ is the normal stress, E is Young's modulus, ε is the normal strain, τ is the shear stress, G is the shear modulus, and γ is the shear strain. The viscous behavior of materials is explained by Newton's law where shear strain is related to the applied shear rate through viscosity. Equation 3 shows Newton's law.

$$\tau = \eta \dot{\upsilon} \qquad \text{Equation 3}$$

Where τ is the shear stress, η is the viscosity, and $\dot{\upsilon}$ is the shear rate. Viscoelastic materials must be described using both Hook's law and Newton's law. Based on the type of material, energy applied due to strain dissipates at different rates (also known as relaxation time). If the material behaves like a solid, energy is stored in the material until it raptures. If the material behaves like a liquid, the energy is dissipated almost instantaneously. Deborah number which is the ratio of relaxation time to the observation time is a good indicator of the material's behavior. Table 2-1 summarizes the relation between Deborah number, type of material, and internal structure.

Table 2-1: Relation between Deborah number, type of material, and internal structure

Deborah number	Type of Material	Internal Structure
>1	Elastic	No change
= 1	Viscoelastic	No significant change
<1	Viscous	Significant change

This study is focused on bentonite suspensions with Deborah numbers greater than or equal to 1. Oscillatory shear tests were conducted to characterize bentonite suspensions' linear and non-linear flow behavior. Oscillatory shear tests show the transformation of bentonite suspensions from gel to solution with increasing shear rates and shear strains. The theory behind oscillatory tests relies in Equations 4 to 6.

$$\gamma = \gamma_o \sin(\omega t) \qquad \text{Equation 4}$$

$$\tau = \tau_o \sin(\omega t + (\delta + \Phi)) = \tau_o' \sin(\omega t) + \tau_o'' \cos(\omega t) \qquad \text{Equation 5}$$

$$\dot{\upsilon} = \gamma_o \omega \cos(\omega t) = \dot{\upsilon}_o \cos(\omega t) \qquad \text{Equation 6}$$

γ_o is the strain amplitude, ω is the angular frequency, τ_o is the stress amplitude, τ_o' elastic stress amplitude. τ_o'' is the viscous stress amplitude, $\dot{\upsilon}_o$ shear rate amplitude, t is time, and δ and

Φ are the phase angles in phase with the strain and strain rate. Oscillatory shear tests subject the specimen to elastic like behavior when the stress and strain occur in phase ($0^\circ < \delta + \Phi < 45^\circ$), and to viscous like behavior when strain lags stress by 90 degrees. ($45^\circ < \delta + \Phi < 90^\circ$). When $\delta + \Phi = 45^\circ$, the material is viscoelastic. Oscillatory tests measure the in-phase elastic modulus G', the out-of-phase viscous modulus G", and the phase angle Φ' as shown in Equations 7 and 8.

$$G' = \frac{\tau o}{\gamma o}\cos(\Phi') \qquad \text{Equation 7}$$

$$G'' = \frac{\tau o}{\gamma o}\sin(\Phi') \qquad \text{Equation 8}$$

Figure 2-4 shows the flow behaviors of various materials. Bentonite suspensions have different flow behaviors based on bentonite concentration. Diluted Na-montmorillonite suspensions (up to 1%) behave like a Newtonian fluid (Kasperski et al, 1986). However, Bandenburg and Lagaly (1988) reported that bentonite suspensions are Newtonian up to 5% solid concentration for shear rate of 200 s^{-1}. For bentonite concentration greater than 5%, the suspensions have a yield stress and show a shear-thinning behavior. The behavior may be modeled by the Herschel Mulkley model (Kelessidis et al., 2007).

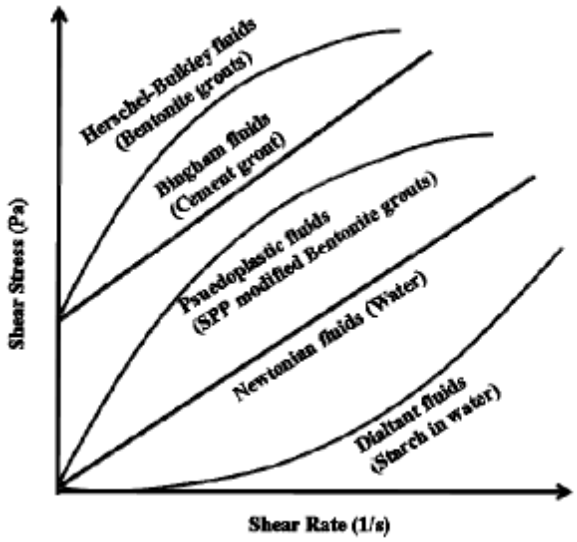

Figure 2-4: Flow of different fluids (Adopted from Yoon, 2011)

2.4.2 Rheometry

Rheometry is used to study the rheological behavior of suspensions. The most common geometries in rheometry are parallel plates, cone and plate, cup and bob, and vane and cup. During this study, the vane and cup geometry was utilized to measure yield stress, viscosity, elastic modulus, viscous modulus, and phase angle. The vane geometry is widely used when testing thixotropic fluids such as bentonite suspensions (Mahaut et al., 2008). The vane is dropped into a cup of bentonite suspensions and rotated at different speeds determined by the applied torque. The shear stress and rate are calculated from the measured torque and rotational speed. The bentonite suspensions in between the vane blades are assumed to be part of the vane and having the shape of a cylinder with a diameter equal to that of the vane. The bentonite is sheared at the boundaries of the cylinder.

The vane and cup geometry is less susceptible to sample disturbance and experimental errors. Sample disturbance is reduced by inserting thin blades into the cup (Barnes and Nguyen, 2001) rather than smearing a lump of bentonite over the area of the base of the plate in the plate-plate and cone-plate geometries. Yoo and El Mohtar (2013) showered that reducing sample

disturbance by using the vane becomes essential when measuring yield stresses over time where using the cone and plate can be under estimating the yield stress by as much as 60%. In addition to reduced disturbance, effects of large particles and wall slip can be neglected because the shearing plane is within the sample (Stokes and Telford, 2004). Nonetheless, the vane geometry is limited to fluids that are not highly affected by the inertia effects because secondary flow and end effect are neglected in this method (Barnes and Carnali, 1990).

2.4.3 Yield stress of bentonite suspensions

Yield stress is the ability of a fluid to resist stress before the initiation of flow. Although there is no general consensus on the definition of yield stress, it is believed that it is due to the fluid's internal structure. Yield stress measurements depend on the measuring system, testing program, and interpretation methods (Nguyen et al., 2006). The measurements also depend on the rest time, shear rate, and type of test performed.

Yield stress in an important parameter in characterizing the strength of bentonite suspensions. Yield stress represents the strength of the network structure formed when the bentonite particles are flocculated in the aqueous medium (Uhlherr et al. 2005). Initial, right after mixing, yield stress measurements provide information on the flow of bentonite suspensions and the yield stress buildup over time can be used to assess their long-term stability post permeation.

Yield stress measurements

The yield stress of the bentonite suspensions was determined by running a stress ramp test using the vane and cup geometry. During the stress ramp test, the shear stress was increased incrementally and the shear stress, shear strain, and viscosity were recorded. Chapter 3 explains

the testing program in details. The magnitude of the yield stress is determined graphically by plotting the shear stress- shear strain on a semi-log scale.

Figure 2-5 shows how to graphically calculate the yield stress. Initially, bentonite suspensions have a solid-like behavior and the shear strain increases at a slow rate as the shear stress increases. Once the yield stress is exceeded, the suspensions act like a liquid and the shear strain increases tremendously causing the stress-strain curve to be almost flat. The yield stress is the intersection point between the two portions of the stress-strain curve (Zhu et al., 2001 and Clark, 2008).

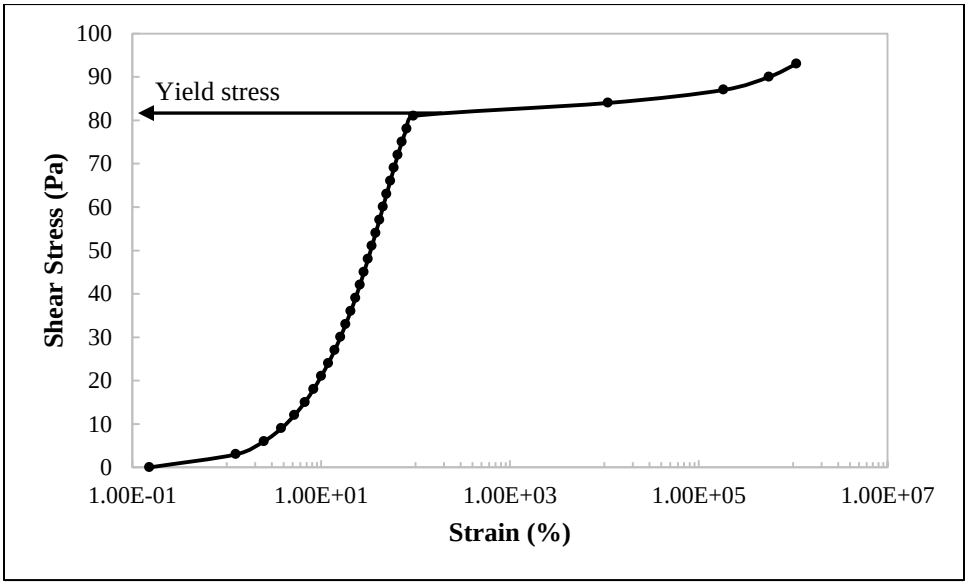

Figure 2-5: Schematically determining yield stress

Yield stress time-behavior

The yield stress of bentonite suspensions is time dependent because of its thixotropic behavior. Bentonite suspensions are at their lowest yield stress when initially sheared during mixing, but the yield stress increases gradually with time. The yield strength increases exponentially at first and then at a slow rate. The vane geometry was used in this study to

properly store the sample in a cup and minimize the effects of sample evaporation. These initial conditions are particularly important immediately after mixing to simulate initial yield stress during the flowing grouting process. It is difficult and impractical to pre-shear the sample and leave it in the rheometer long periods of time. Therefore, samples are stored in separate cups and tested at desired times. Disturbance due to vane insertion and evaporation are minimized.

2.5 Permeation

Under seepage may be mitigated through permeation, also known as grouting. Granular soil deposits are injected with engineered fluids which are less permeable through pressure injection in boreholes. A grout curtain wall is constructed vertically to build an impermeable barrier. According to Karol (2003), at least three rows of holes are required to approach complete cutoff and the distance between them ranges from 1 to 5 feet. Permeation grouting is a non-destructive method that creates minimal ground disturbance and so can be used for in situ remediation to existing structures. However, the success of the seepage wall depends on the treated soil and the compatibility between the soil and grout. Similarly, the injection pressure or flow rate depends on the soil type, depth of injection, confining soil and structural pressure. It is difficult to predict the penetration distance and flow of grout in heterogeneous soils because the flow follows the path of least resistance.

There are two types of injection materials; particulate and chemical grouting. Particulate grouting includes bentonite and cement which is composed of water and Portland cement. Chemical grouts include resins and other polymers which are capable of penetrating finer grained soils which are inaccessible to particulate grouts. Cement and chemical grouting cause groundwater contamination due to long term reaction with it (Metcalfe and Walker, 2004); therefore, bentonite has proven to be an environmental friendly and long term safe alternative.

The background on permeation grouting is presented in this section to understand the formation of bentonite-sand mixtures. Cement and soil groutability criteria, and grout flow and stoppage are discussed to comprehend factors affecting the permeability of bentonite into sand including bentonite particle size, sand particle size, and yield stress.

2.5.1 Soil groutability criteria

The most common form of grouting is cement grouting; therefore, most of the literature available is on cement grout criteria. The larger particle sizes of the grout and the size of voids in the grouted sands (mostly related to the smaller particle sizes of the sand) are the two most important factors affecting permeability. Burwell (1958) suggested that the groutability parameter N be the ratio of d_{10} of grouted soil to d_{95} of the grout as shown in Equation 9.

$$N = \frac{d_{10}}{d_{95}} \qquad \text{Equation 9}$$

N is the permeability number, d_{10} is the diameter of soil passing 10% total soil mass (grouted soil), and d_{95} is the diameter of soil passing 95% of total soil mass (grout). The soil can be easily grouted is N is greater than 11, and not groutable for N less than 5.

Karol (2003) linked groutabilty criteria to hydraulic conductivity and grain size distribution. The latter two are closely related.

Table 2-2 and Figure 2-6 show relationship between groutabilty and hydraulic conductivity and groutability and grain size distribution respectively.

Table 2-2: Relationship between hydraulic conductivity and groutablity (Adapted from Karol, 2003)

Permeability (cm/sec)	Groutability (Ability of the soil to receive grout)
$\leq 10^{-6}$	Ungroutable
10^{-5} to 10^{-6}	Groutable with difficulty by grouts with viscosity < 5 mPa • s and ungroutable with grouts having a viscosity > 5 mPa • s
10^{-3} to 10^{-5}	Groutable with low viscosity grouts but difficult with grouts with a viscosity greater than 10 mPa • s
10^{-1} to 10^{-3}	Groutable with all commonly used chemical grouts
$\geq 10^{-1}$	Requires suspension grouts or chemical grouts containing a filler material

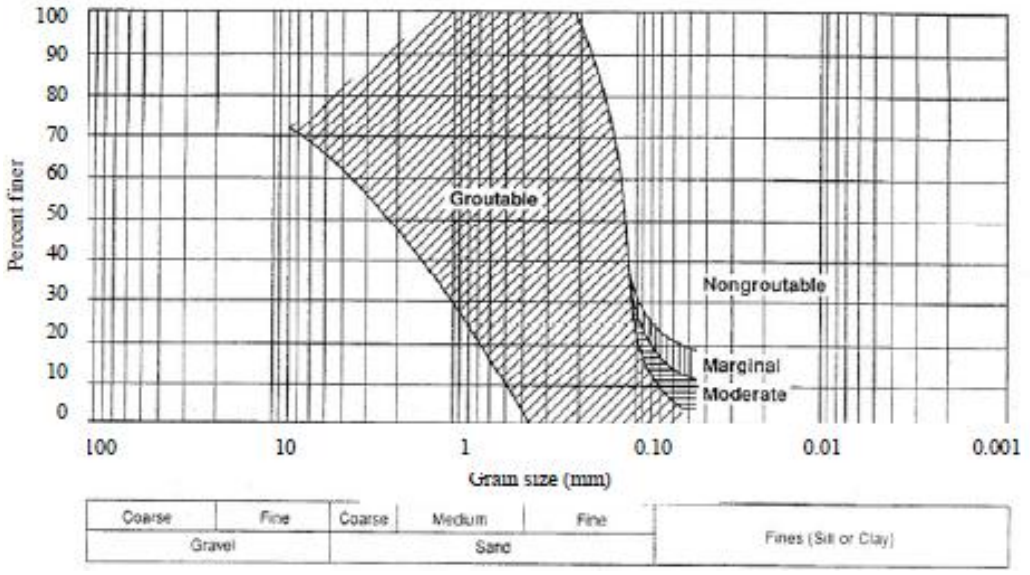

Figure 2-6: Grain size distribution suitable for grouting (Adapted from Karol, 2003)

Further research was conducted and it was found that fine contents (FC), grouting pressure (P), and relative density (Dr), and water cement ratios (W/C) also affect the permeability of grout into sand (Akabulut and Saglamer, 2002). It is important to know the penetration distance of grouts into grouted soil to understand the extent of the grouted area. The

factors that govern permeability are the same as those that govern penetration distance, in addition to yield stress and viscosity (Santagata and Santagata, 2003).

Work by Yoon and El Moohtar (2013) on groutability of SPP modified bentonite suspensions showed that the groutability of bentonite suspensions depends on effective grain size, relative density, fines content, apparenty viscosity, and injection pressures (Equation 10).

$$N* = N_c + \Phi_1 \frac{\left(\frac{P}{1atm}\right)^{\Phi_2}}{(\mu_r)^{\Phi_3}} + \left(\frac{Dr}{100}\right)^{\Phi_4} - e^{\left(\Phi_5 \frac{FC}{100}\right)} \quad \text{Equation 10}$$

Where N* is the groutablity of bentonite suspensions, Φ_1, Φ_2, Φ_3, Φ_4, and Φ_5 are the empirical constants, P is the injection pressure (kPa), μ_r is the relative viscosity at the equilibrium shear rate (μ_{grout} (mPa·s)/ μ_{water} (mPa·s)), FC is the non-plastic fines content in granular soils (%), and N_c is the normalized effective grain size of sand (d_{10},sand (mm) / d_{95} ,bentonite (mm)). Table 2-3 summarizes the empirical parameters. Based on this criterion, a soil is groutable if N* is greater than 11 and not groutable if N* is less than 9. It is recommended to conduct a trial grouting in the laboratory if the N* is between 9 and 11. The proposed correlation is reasonable between the following intervals: 5 ≤ bentonite fraction ≤12%, 0 ≤ SPP ≤ 4%, 4.8 < Nc < 12.6, 30 ≤ Dr ≤ 80%, 0 ≤ FC ≤ 15%, k ≥ 0.01 cm/s and P ≤ 140 kPa (Yoon and El Mohtar, 2013).

Table 2-3: Empirical parameters used in groutablity equation (Yoon and El Mohtar (2013))

Φ_1	Φ_2	Φ_3	Φ_4	Φ_5
1900	0.2	1.4	8.5	9.3

2.5.2 Grout flow and stoppage

The flow of grout in porous medium and its stoppage mechanism contribute to understanding the theory behind penetration distance. Filtration is a process that allows grout to

flow into the pores of soils until the flow path is blocked. Saada et al. (2005) summarized four different approaches used to explain filtration; however, all of the approaches are based on constant flow rate conditions. In this study, constant pressure was used to study the penetration length of bentonite suspensions into sand, while constant flow was used to permeate the sand with bentonite for the washing out tests. A 3-D step-wise model was developed to correlate groutability to the parameters affecting it. Darcy's law and Kozey-Carman equation are considered in the model to adjust for porosity and volumetric flow during filtration.

Grout flows into the grouted soil as long as the injection pressure is greater than the resistance in the soil. Once the shear stresses developed in the suspension due to the applied pressure are less than those required to generate flow at a given shear rate (equivalent to the flow rate), the grout flow stops. Filtration also stops the grout flow when the flow path is blocked. Flow is highest at the beginning and then slows down as more paths are blocked. According to Herzig et al. (1970), filtration governs the grout flow stoppage which results in different penetration distance. On the other hand, grout flow stoppage can be explained by the clogging mechanism. Clogging occurs when the particles of the grout cannot enter the grouted soils pores. This occurs when the grain size of the grout is a third or greater than the size of grouted sand pores (Axelsson et al., 2009).

2.6 Hydraulic Conductivity

A hydraulic conductivity of at least $1x10^{-7}$ cm/s is generally required for water and waste containment liners (Chalermyonant and Arrykul, 2005). Consequently, Sand permeated with bentonite suspensions were studied and accordingly proved to be efficient containment liners. They have a hydraulic conductivity ranging between 10^{-6} to 10^{-9} cm/s depending on the bentonite content.

2.6.1 Hydraulic conductivity of Sand permeated with bentonite suspensions

Granular material have a relatively highly hydraulic conductivity; therefore, bentonite is mixed with it to enhance the hydraulic performance. Grouted bentonite reduces the hydraulic conductivity of soils with hydraulic conductivity of 0.1 to 1 cm/sec by two orders of magnitude (Karol, 2003).

Hwang (2010) stated that 8% bentonite content by mass reduced the hydraulic conductivity of a sand with a clean hydraulic conductivity of around 10^{-2} cm/s up to 10^{-9} cm/s. When 5% dry bentonite (by mass of sand) was mixed with sand, the hydraulic conductivity of clean sand was reduced to 10^{-6} cm/s (Chapius, 2002). Yoon; (2011) reported that the hydraulic conductivity of Ottawa sand decreased by 3 to 7 orders of magnitude depending on the bentonite content in the sand as shown in Figure 2-7 where the hydraulic conductivity of the Sand permeated with bentonite suspensions is normalized by the hydraulic conductivity of the clean Ottawa sand. Abichou et al. (2000) confirms Yoon's results by stating that the hydraulic conductivity of compacted sand bentonite mixtures was reduced up to 6 orders of magnitude when bentonite contents of 5 to 16% were used.

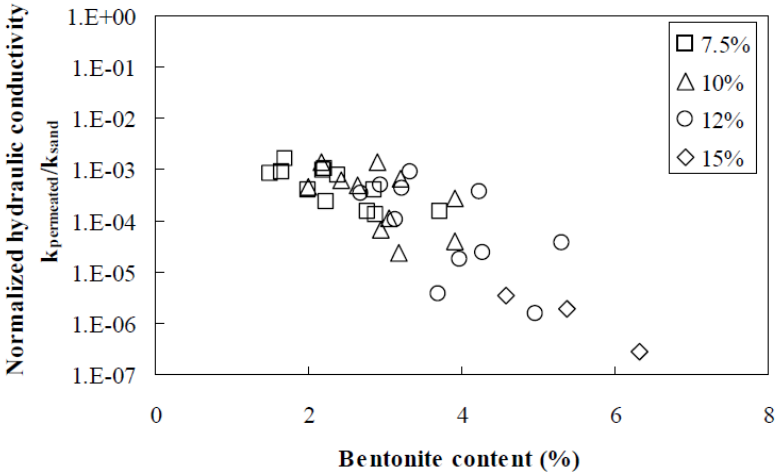

Figure 2-7: Normalized hydraulic conductivity based on bentonite content (Adapted from Yoon, 2011)

2.6.2 Degree of saturation

The degree of saturation may be a source of error during the measurement of hydraulic conductivity. As the degree of saturation decreases, the hydraulic conductivity decreases because the flow paths are blocked by the air bubbles. And so, it is crucial to achieve full saturation to eliminate low misleading hydraulic conductivities. The samples are exposed to air while being prepared in the laboratory, and even though deaired water and watertight equipment are used, the equipment is not airtight (Hwang, 2010). Flushing the specimen with carbon dioxide (CO_2) before flushing it with water and applying vacuum during water flushing are most common methods to increase the degree of saturation. Another reliable saturation method is applying backpressure which was used during this study.

2.6.3 Clay void ratio

The hydraulic conductivity of sand-fine mixture highly depends on the void ratio of the mixture; therefore, it is important to determine the appropriate void ratio during sample preparation and analysis. Void ratio also known as bulk void ratio is defined as the ratio of volume of voids; air and water, to volume of solids. Although the volume of fines in sand is

considered as part of the total volume of solids, it actually should be added to the volume of voids because permeation grouting occurs in suspension form, hence occupying pore volume. Skeletal void ratio e_G takes into consideration this assumption and is defined as follows (Mitchell, 1993):

$$e_G = G_s \frac{\frac{W}{100} + \frac{FC_c}{100G_{sC}}}{1 - \frac{FC_c}{100}} \qquad \text{Equation 11}$$

Where G_s and G_{sC} are the specific gravities of the clay and the granular particles respectively, W is the water content (%), FCC is the percentage of clay to total solids by dry weight (%).

When the skeletal pores are filled and blocked with sufficient amount of bentonite, water tends to flow through the clay voids rather than skeletal pores (Castelbaum and Shakelford, 2009). Clay void ratio (e_b) is defined as the volume of voids attributed to the bentonite divided by the volume of solid bentonite in the mixture (Kenny et al., 1992) as expressed in the following equation:

$$e_b = G_{sb}\left[\left(1 + \frac{1}{r}\right)\frac{\rho_w}{\rho_{dm}} - \frac{1}{rG_{ss}}\right] - 1 \qquad \text{Equation 12}$$

Where G_{sb} and G_{ss} are the specific gravity of bentonite and sand respectively, r is the ratio of dry sand to bentonite, ρ_w and ρ_{dm} are the density of water and dry density of the mixture respectively.

The hydraulic conductivity of sand permeated with bentonite suspensions depends on the characteristics of the pore spaces; clay void ratio and the bentonite content. Yoon; 2011

developed a relationship shown in Figure 2-8 between the hydraulic conductivity, clay void ratio, and bentonite content normalized by the maximum bentonite content. The hydraulic conductivity tends to decrease rapidly as the clay void ratio decreases when the bentonite content is greater than 3%; however, the change in hydraulic conductivity with bentonite content is less significant when the bentonite content is less than 3%.

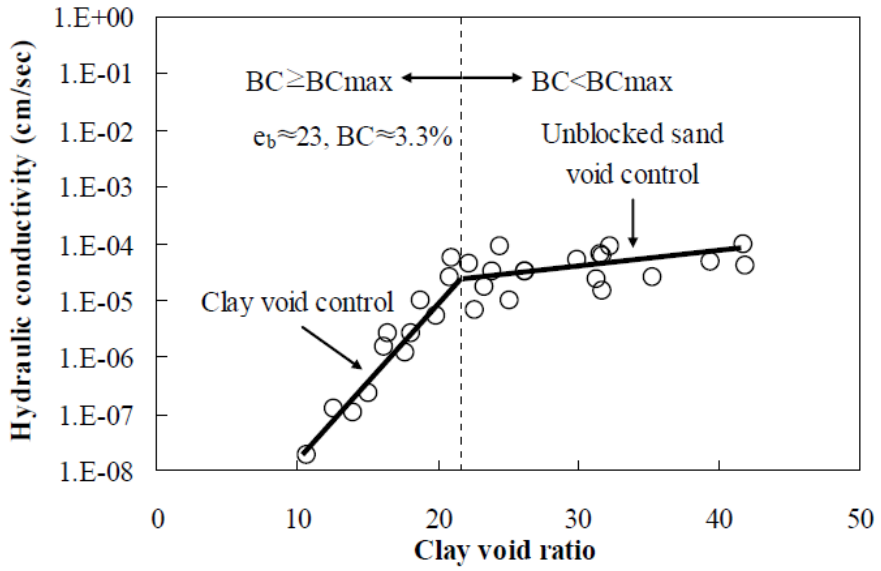

Figure 2-8: Variation of the hydraulic conductivity of Ottawa sand with clay void ratio and BC/BCmax

2.7 Stability of Sand permeated with bentonite suspensions

Once sand-bentonite walls have been constructed, it is important to evaluate the stability and long-time performance of these walls. Sand permeated with bentonite suspensions fail when the bentonite particles washout causing the hydraulic gradient to increase beyond the minimum requirement for a hydraulic conductivity of 10^{-7} cm/s.

2.7.1 Shear strength of Sand permeated with bentonite suspensions

This study is based on a main assumption that the shear strength of the original sand is slightly and insignificantly changed when permeated with bentonite. Rugg et al. (2010) studied

the effect of bentonite permeating on shear strength by performing consolidated-undrained tests on permeated sand specimens. Tests conducted on 10% bentonite suspensions with 2% SPP showed that the friction angle of the permeated sand at the critical state and undrained instability state did not change significantly when permeated with bentonite suspensions.

2.7.2 Stress Distribution

The yield stress of bentonite suspensions is the threshold stress after which the suspensions are mobilized. Therefore, the distribution of the stresses applied on the bentonite suspensions within the sand network under a given hydraulic flow conditions can provide information on the stability of the sand permeated with bentonite suspensions. Abichou (2004) developed a network formulation to model the hydraulic conductivity of sand permeated with bentonite suspensions. The sand particles were assumed to be spheres arranged in the form of neighboring tetrahedrons. The pores were assumed to be capillary tubes with diameter and lengths defined by the tetrahedrons' geometry. The diameter of the pores assumed to be capillary tubes can be estimated in two methods; estimating the effective radius or the equivalent radius. The effective radius is also known as the arithmetic mean of the radius of the largest circle between spheres surrounding a pore. The equivalent radius is defined as the radius of an equivalent area to the pore space between the adjacent spheres (Bryant et al, 1993). Figure 2-9 is a schematic diagram of the two capillary tubes assumed to estimate the radius of the pores.

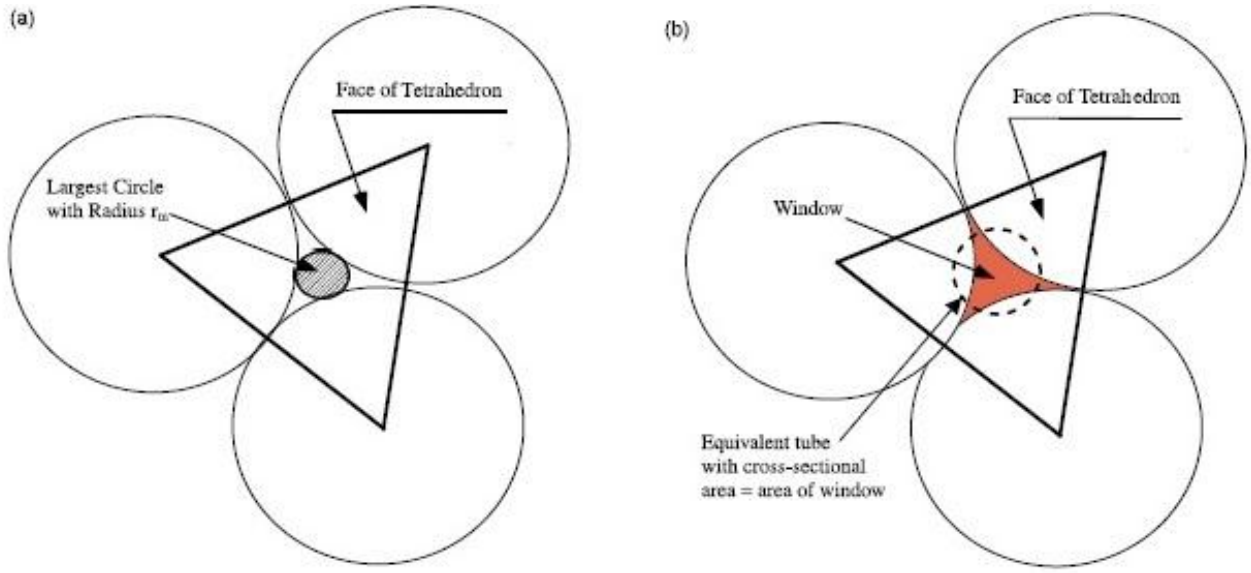

Figure 2-9: Schematic diagram of (a) largest circle with effective radius and (b) equivalent circle (Adapted from Abichou et al, 2004)

The stress applied by the bentonite suspensions on the sand network can be estimated once the radius of the pores is known. The general equation for predicting stresses applied in a capillary tube during flow (Equation 13) is used.

$$\tau = \frac{P_2 - P_1}{2L} R_{eff\ or\ eq} \qquad \text{Equation 13}$$

Where τ is the stress applied, P_2 and P_1 are the pressures applied at the top and bottom of the sand permeated with bentonite suspensions sample respectively, L is the length of the sample, and $R_{eff\ or\ eq}$ is the effective radius or equivalent radius.

2.7.3 Post grouting stability

Sand permeated with bentonite suspensions must remain stable under gravity settling and hydraulic gradient. Camberfort (1964) proposed a sample equation (Equation 14) to estimate the minimum pressure gradient needed to washout the bentonite. The pressure gradient is closely

related to the yield stress of bentonite; therefore, the rheological properties of bentonite were well studied

$$\frac{P}{L} = \tau_0 . S . (1 - n) \qquad \text{Equation 14}$$

Where P is the pressure gradient (Pa), L is the length of the grouted zone (m), τ_0 is the yield stress (Pa), S is the specific surface of soil (1/m), and n is the porosity of the soil.

Darcy's law governs the water flow through Sand permeated with bentonite suspensions since the hydraulic gradient is linearly proportional to the flow rate. The bentonite content (ratio of bentonite to sand by dry mass) and its distribution in Sand permeated with bentonite suspensions highly affects the mixtures' hydraulic conductivity. The mixture is more homogenous when the bentonite content increases (Borgesson et al., 2003), and the effects on the hydraulic conductivity are reduced because the flow path are smaller and more circuitous (Chapuis, 2002). The washing out of bentonite can be detected by applying excessive hydraulic gradients which mobilize bentonite and consequently significantly increasing the hydraulic conductivity (Kaoser et al, 2006). Bentonite washouts more easily in mixtures with low bentonite content because the water flows through the sand voids which have not been blocked by bentonite (Koaser et al., 2006).

CHAPTER 3: EXPERIMENTAL PROGRAM

3.1 Introduction

The experimental program includes the material properties, equipment, and setups used in this study. Sand, bentonite, granular filter material, and water utilized throughout the experimental work were characterized by Yoon, 2011. The rheological, permeation, and washout setup are the three components of the experimental program for this study. The rheometer setup was used to determine the rheological properties of freshly prepared bentonite and over extended times. The permeation setup was used to permeate the sand samples with bentonite. Based on that, Yoon's (2011) empirical equation to predict the penetration depth of bentonite into sand was modified to accommodate for permeameters with varying diameters. As for the washout setup, its purpose was to evaluate the stability of bentonite suspensions in Sand permeated with bentonite suspensions. Hydraulic conductivity tests were conducted at increasing hydraulic gradients to determine the point of washing out. This section also includes the calibration of the differential pressure transducers used to record flow volume and head difference with the help of a data acquisition system.

3.2 Material Properties

The physical properties of all the materials used were analyzed. Moreover, the chemical properties and composition of bentonite was analyzed to fully understand its behavior.

3.2.1 Sand

Ottawa (ASTM graded C778) sand was used to study the penetration of bentonite suspensions through permeable sand and the washing out of bentonite due to varying hydraulic gradients. Grain size distribution was determined by sieve analysis based on ASTM D422-63;

whereas, the specific gravity and maximum and minimum void ratio were determined in based on ASTM D854-02, D4253 and D4254, respectively. Ottawa sand is classified as SP based on USCS classification with little to no fines. Table 3-1 summarizes the index properties of Ottawa sand; whereas, Figure 3-1 shows the grain size distribution curve (Hwang, 2010).

Table 3-1: Index properties of Ottawa sand

Sand	Gs	e_{max}	e_{min}	D_{10} (mm)	D_{30} (mm)	D_{60} (mm)	Cu	Cc	USCS
Ottawa	2.65	0.76	0.5	0.2	0.32	0.4	1.94	1.28	SP

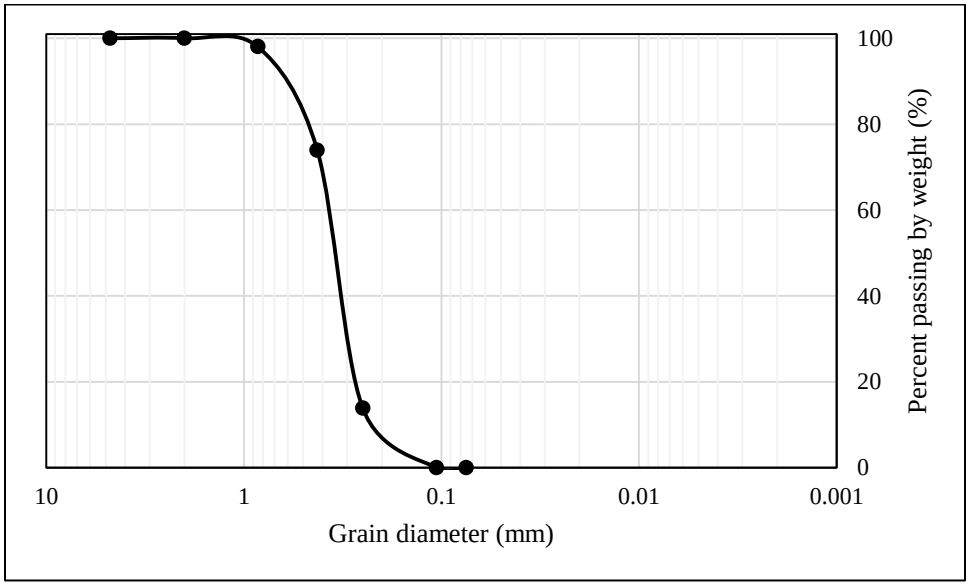

Figure 3-1: Grain size distribution curve for Ottawa sand

3.2.2 Bentonite

The bentonite used in this study is high swelling Wyoming bentonite powder (Volclay CP-200) obtained from CETCO. Yoon (2011) characterized in details the Wyoming bentonite powder, including particle size, X-ray diffraction, Atterberg limits, activity, specific gravity, cation exchange, energy dispersive X-ray Spectroscopy (EDX), and pH measurements. This bentonite is commercially used for the construction of sand/bentonite slurry trench walls. It has a

maximum filtrate loss of 18 ml, a barrel yield of 90 minutes based on API 13A, and a free swelling capacity up to 16ml/2g when fully hydrated.

Particle Size

Permeation grouting is highly dependent on the bentonite particle size; therefore, it is important to reduce the effects of impurities present in the commercial Wyoming bentonite. Accordingly, the bentonite was sieved with a No.200 (>75 μm) sieve. The sieved bentonite particle size was characterized using hydrometer tests performance in accordance with ASTM D422. A dispersing agent (sodium hexametaphosphate, 10% by dry weight of bentonite) and high shear mixing were needed during testing to control bentonite's high tendency to flocculate. The sieved bentonite has 95% of particles less than 25μm, 60% of particles less than 2μm and 50% of particles less than 1μm (Yoon, 2011). Figure 3-2 shows the grain size distribution curve for the sieved bentonite.

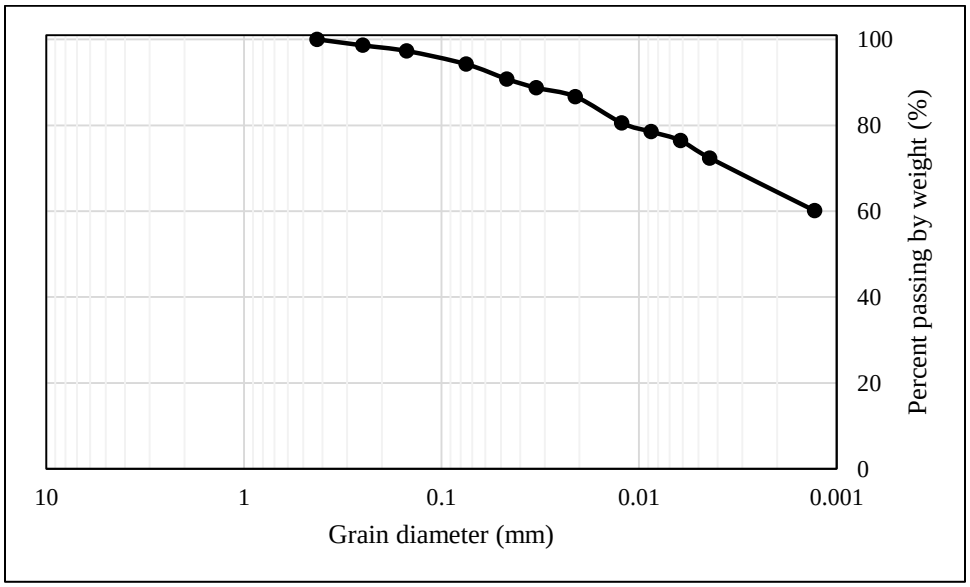

Figure 3-2: Grain size distribution curve for the sieved bentonite

X-ray diffraction and Atterberg limits

X-ray diffraction (XRD) was performed on the bentonite to provide information on the distribution and crystalline structure of the minerals present in the sample. The XDR tests conducted on sieved bentonite identified the presence of quartz, feldspar, mica, and montmorillonite. Moreover, the bentonite's Atterberg limits were determined to further identify the minerals based on the plasticity chart developed by Casagrane (1948). The Atterberg limit tested were performed in accordance with ASTM D4318. The sieved bentonite has a liquid limit of 440% and plastic limit of 40% (Yoon, 2011).

Activity and pH measurement

Activity is a property that indicates the behavior of clay. Higher activity implies that the clay is likely to be affected by the physiochemical factors such as exchangeable cations and pore-fluid compositions. The sieved bentonite has an activity of 4.8 which is within the range of activity for Na-Montmorillonite of 4-7 (Haltz and Kovacs, 1981).

The pH of bentonite suspensions affects the particle associations which consequently affects their flow behavior (Kelessidis et al. 2007). The average pH of the bentonite suspensions is 9.33 with a standard deviation and C.O.V. of 0.21 and 0.02, respectively. This proves the consistent alkalinity of the suspensions (Yoon, 2011).

Specific Gravity (Gs) and Specific surface area

Previous research reported specific gravity values within a range of 2.35 to 2.88 (Komine and Ogata, 2003; Kaoser et al., 2006). The average specific gravity of the sieved bentonite was 2.64 which has been measured in accordance with ASTM D-854-02 using a 250 ml volumetric

flask (Yoon, 2011). On the other hand, the bentonite's specific surface area was measured to be 712.5 m^2/g which falls within the typical range of 400 to 800 m^2/g (Santamarina et al., 2002).

3.2.3 Sodium pyrophosphate decahydrate

Sodium pyrophosphate (SPP) decahydrate ($Na_4P_2O_7 \cdot 10H_2O$) powder with 99% purity was purchased from Sigma-Aldrich Inc. The used SPP is a nontocix, white, odorless, and crystalline material. It has a solubility of 62 g/l at 20˚C, specific gravity of 1.82, and molecular weight of 446.06. The pH of an SPP solution of concentration 1 to 5% ranges between 9.5 and 10 (Clarke, 2008).

3.2.4 Water

The properties of bentonite are altered when mixed with water; therefore it is important to determine the ionic strength of mixing water. The electric conductivity of 3 types of water; tap, pure, and de-ionized, was measured using a CDM230 conductivity meter at the University of Texas at Austin. Although it is not practical to use de-ionized water in the field, de-ionized water with pH of 6 was used in this study. Table 3-2 summarizes the ionic strength of the water.

Table 3-2: Ionic strength of water

Water type	**µm/cm**	**mM**
Tap	335	$4.6x10^{-3}$
Pure	0.83	$1.1\ x10^{-5}$
De-ionized	0.96-1.56	$1.3\text{-}2.2\ x10^{-5}$

3.2.5 Filter Materials

Fine aggregate and coarse sand were used in the experiment setup to create a uniform distribution of bentonite suspensions during its permeation through sand. The fine aggregate (pea

gravel) with diameter > 4.75m was sieved though the No.4 sieve; whereas, the coarse sand with 1.2mm< diameter < 1.75mm was sieved through No.10 sieve and retained through No.16 sieve.

3.3 Equipment and Setup

The experimental equipment and setup for this study are presented in this section. The study involved three setups: the rheological setup, permeation setup, and the washing out setup.

3.3.1 Rheological setup

The rheological setup describes the Rheometer utilized during this study, sample preparation process, and testing procedure.

Rheometer

The Physica MCR 301 rheometer manufactured by Anton Par was used in this study. The rheometer has the dimensions of H×W×D of 62.1cm×48.5cm×60.3cm. There are many tests that can be performed using the rheometer. Two types of tests were conducted during the study: strain sweep and stress ramp tests. These tests are oscillatory, monotonic, stress-controlled (stress ramp), and strain-rate controlled (strain sweep). An automated computer software, Rheoplus, was programmed for testing the bentonite suspension samples prepared during the study. The rheometer has four measuring systems including the parallel plate, cone and plate, bob and cup, and vane and cup.

During this study, the cone and plate and vane and cup measuring systems were used. Bentonite suspensions test results from the cone and plate and vane and cup were compared. However, the rheological properties of bentonite were characterized using the vane and cup measuring system to minimize disturbance and the ability to store bentonite suspensions in cups. The bentonite suspensions were stored in cups to study the time behavior rheological properties.

The vane has six 1-mm thick and 16mm long blades and has a radius of 11mm. The cup is 80mm in length and has an internal diameter of 29mm. As for the cone and plate, both have a diameter of 50mm and the cone has an angle of 1º. Figure 3-3 shows the rheometer setup with the vane and cup measuring system.

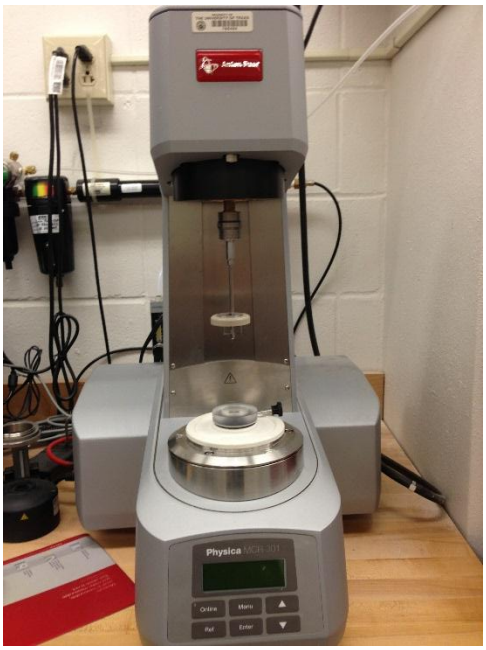

Figure 3-3: Rheometer setup with vane and cup measuring system

Device initialization and setup

The MCR 301 rheometer needs to be initialized before the tests are run. A pressure level of approximately 80 psig is supplied to feed the air bearing from an external barometer. Once the pressure level is adjusted, the temperature of the location where the specimen is placed is adjusted using a Peltier temperature control regulated by Rheoplus. A water bath connected to the back of the rheometer keeps the temperature constant at 22ºC which is the temperature used in this study. Afterwards, the device is initialized by clicking on the "Initialize" button on the Rheolpus software. The latter checks the gap and rotor sensors by moving the measuring head to the top position and then rotating it at high speed. Upon the completion of the initialization

process, the measuring system is mounted to the motor coupling and it is automatically identified through a smart chip system.

For the cone and plate measuring system, the lift position is adjusted at a 140mm; whereas, the measure position (also referred to as "zero gap") is at 0.093 mm (the gap is between the cone and the plate). A few drops from the bentonite suspensions sample are placed on the plate. Once the cone is dropped to the zero gap reference point, some of the suspensions on the plate are expelled outwards. With extreme care, the suspensions are trimmed with a flat-bladed spatula. This is done to reduce inaccuracy in the results. Finally, the rheology testing begins by hitting the "Start" button on the Rheoplus software after the desired loading sequence has been programmed.

For the vane and cup measuring system, the lift position is adjusted at 180mm; whereas, the measure position is at 0 mm (the vane is still in the center of the bentonite in the cup and not at the bottom of it). The cup, filled with bentonite suspension, is placed in position on the rheometer. Note that the bentonite suspensions are poured into the cup immediately after preparation. The vane is dropped into the measure position (where it is completely immersed in the sample, but far enough from the base of the cup to eliminate end effects) and the test begins once the "Start" button is pressed.

Testing program

The experimental program in this study involved two types of testing mechanisms; stress ramp and strain sweep. Stress ramp testing was used to determine yield stress and equilibrium viscosity; whereas, the oscillatory shear testing was used to find the storage/loss modulus and phase angle.

Stress ramp

The stress ramp technique is selected for this study to provide a consistent way of measuring low and high yield stresses. This method allows yield stresses and apparent viscosities to be estimated at a large range of shear rates. The test program is set up as to allow the sample to rest for 2 minutes before the first stress is applied. The resting time is designated to provide consistent initial conditions for all tests. Afterwards, the stress level is increased at a rate of 0.25 Pa/s. Each stress level is sustained for 12 seconds and then increased at a rate of 3 Pa/step.

Several stress ramps were tested before selecting the rate of 3 Pa/step because the ramp rate should be slow enough to detect the yield stress of low concentration bentonite suspension concentrations (Zhu et al., 2001). However, Yoon (2011) reported that very slow stress ramps might be erroneous for bentonite suspensions with large stresses due to evaporation from sample surface and edge in the vane and cone measuring systems, respectively. For freshly prepared 5% concentration of bentonite suspensions, slow ramp rates of 1 and 2 Pa/step produced yield stress less than that outputted for 3 Pa/step. Whereas, the freshly prepared 7.5% concentration of bentonite suspensions had almost identical yield stresses for ramp rates of 1, 2, and 3 Pa/step (Yoon, 2011). Accordingly, the stress rate of 3Pa/ step is selected since bentonite suspensions of 7% or more were to be tested for this study.

Strain sweep

The strain sweep tests were performed to understand the behavior of bentonite suspensions under dynamics loading. Oscillatory strains are applied at increasing amplitudes and constant frequency. The test outputs the elastic storage modulus G’ which is in phase, and the viscous component G’’ which is out-of-phase with the applied strains. The critical storage

modulus and critical strain are determined at the intersection point of the linear and nonlinear behavior of the bentonite suspensions. The linear elastic behavior is observed at small strains as a plateau where the storage modulus G' is constant. The nonlinear viscoelastic behavior is depicted as the downward sloping curve at higher strains. Beyond the critical strain, the storage modulus G' decreases; whereas, the loss modulus G'' and phase angle increase as shown in Equations 4 to 6. Figure 3-4 shows the storage modulus G', loss modulus G'', and phase angle δ versus strain.

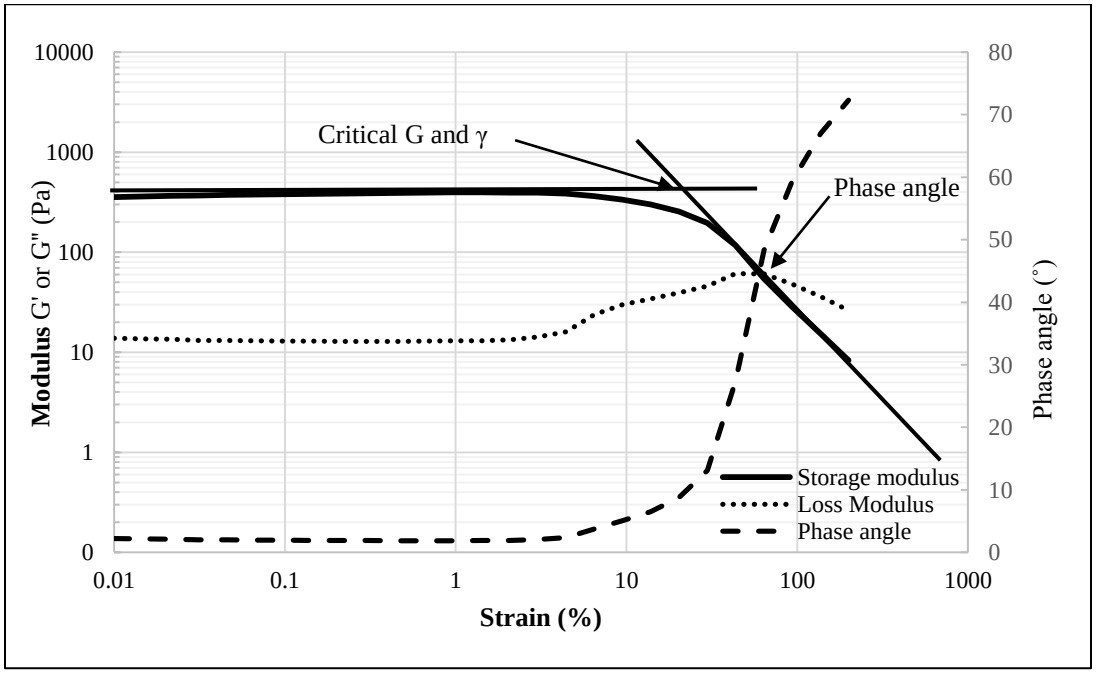

Figure 3-4: Storage modulus, loss modulus, and phase angle from strain sweep test

The oscillatory shear test were performance at a frequency of 1Hz and strain ranging from 0.01% to 1000%. Initially, the sample is allowed to rest for 2 minutes while being tested at a strain of 0.01%. Afterwards, the strain is increased at a logarithmic rate such that 6 data points are recorded per log cycle. The tests were conducted at a constant frequency because bentonite suspensions' rheological properties are independent of frequency (Geier, 2004).

Preparation of bentonite suspensions

Samples of bentonite suspensions were prepared for studying the rheological properties of bentonite. Unmodified suspensions and sodium pyrophosphate decahydrate modified suspensions were prepared. The Wyoming bentonite used in this study has an initial water content of 8.2%. This water content was taken into account to determine the accurate weight of bentonite and SPP (for modified suspensions) needed to achieve suspensions with desired concentrations. The calculations were based on the mass fraction of dry bentonite by total mass of suspension for bentonite content and mass od SPP by dry mass of bentonite for SPP concentration.

Unmodified suspensions

The detailed sample preparation of unmodified bentonite suspensions is described in the following step by step procedure:

1. Place some of the sieved bentonite in a bowl to avoid exposing all of the sieved bentonite to room humidity which might alter the bentonite's water content.
2. Place a mixing cup on a weighing scale and tare to zero.
3. Add de-ionized water to the cup till half of the total suspensions weight is reached. i.e., add 175g of de-ionized water for a sample of 350g.
4. Add the needed amount of sieved bentonite to the cup.
5. Add de-ionized water to the cup till the total weight of suspensions is reached.
6. Place the mixing cup in a high shear mixer and let it mix for 5 minutes as shown in Figure 3-5.

7. Remove the cup from mixer and manually scrape the sides and base to allow uniform and consistent suspensions to be prepared.
8. Place mixing cup in mixer and repeat step 7 two more times.

Figure 3-5: Mixing cup with bentonite suspensions on mixer

SPP modified suspensions

The sodium pyrophosphate decahydrate modified suspensions were prepared in a similar manner; however, the detailed procedure is described as follows:

1. Place a mixing cup on a weighing scale and tare to zero.
2. Add the amount needed de-ionized water to the cup.
3. Add the amount of SPP solution to the mixing cup by using a dropper.
4. Mix the water and SPP solution in the mixer at high shear for 5 minutes.
5. In another mixing cup, place the mixed water and SPP solution and add the needed amount of sieved bentonite to the cup.

6. Place the mixing cup in a high shear mixer and let it mix for 5 minutes.
7. The remaining mixing process is similar to that of the unmodified bentonite suspensions.

Storage of bentonite suspensions

The rheological properties of bentonite suspensions over time were studied to fully understand the behavior of bentonite. The vane and cup measuring system was used to minimize disturbance to the sample. After bentonite suspensions are freshly prepared, bentonite is poured into the cups till the 37ml mark is reached. 37ml was selected as an appropriate volume of bentonite suspensions so that the blade would be immersed in a depth twice its length. Each cup is covered with a paper towel and plastic wrap tightly wrapped with an elastic band. The paper towel is placed on top of the sample to label it with information about the sample. Such information includes the bentonite suspensions concentration, the date at which the sample should be tested, and numbers of days after preparation. The samples were stored in an isolated area to minimize disturbance from vibration and shaking. Figure 3-6 shows bentonite suspension samples stored and labeled.

(a) (b)

Figure 3-6: (a) Empty cup, (b) bentonite suspensions stored, covered, and labelled

3.3.2 Permeation setup

This section describes the permeation setup used to modify Yoon's (2011) empirical equation to estimate the penetration depth of bentonite into sand and in preparing samples for the washout tests.

Sample preparation

Four permeameters were utilized to test Yoon's (2011) empirical equation for estimating the penetration depth of bentonite. All permeameters were transparent to detect the flow of bentonite suspensions through the sample. Figure 3-7 shows the permeameters used in this study, and Table 3-3 summarizes the outer diameter, and inner diameter, and height of the permeameters used during this study.

(a)

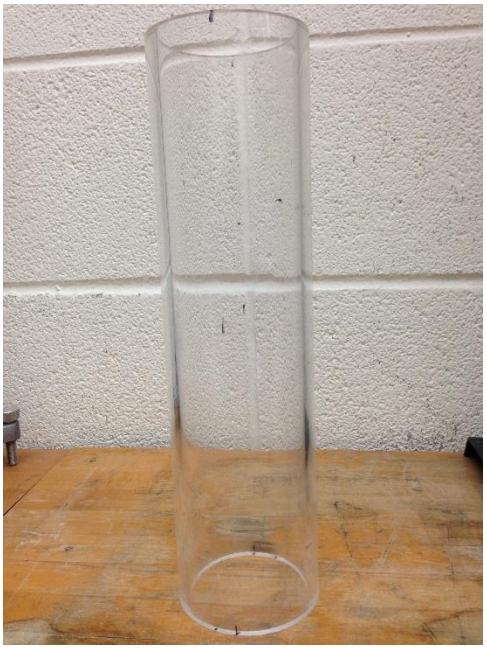

(b)

(c) (d)

Figure 3-7: (a) Permeameter 1, (b) Permeameter 2, (c) Permeameter 3, and (d) Permeameter 4

Table 3-3: Summary of permeameters' outer diameter, inner diameter, and height

Permeameter	Outer diameter (cm)	Inner diameter (cm)	Height (cm)
1	5.1	3.8	21.6
2	8.1	7	20.5
3	6.1	10.2	9.7
4	15.2	14	37

For all permeameters, a 2.5 cm thick layer of filter material; gravel and coarse sand, was placed at the bottom and top of the sample. The bottom filter material's role is to provide uniform distribution of the bentonite suspensions across the area of the sample; whereas, the top layer is placed to prevent the washing out of sand. For consistency, the gravel and the coarse sand were each 1.25 cm thick. Ottawa sand was deposited on top of the bottom filter layer using a scoop and funnel. Although the effect of density on the penetration equation and washing out is minimal, the sample was tapped to achieve a relatively density of 50% to reduce discrepancies in the results. Sand was added to the permeameter until 2.5 cm were left at top for the filter material

to be added. After the permeameter is tightly closed, the sample is saturated with water by flushing the sample with de-ionized water equal to at least 3 times its pore volume. The sample is flushed with more water at a pressure of 35 kPa to expel possibly trapped air bubbles.

Permeation process

The permeation setup consists of the permeameter described earlier, a pressure cell, pressure panel, and a balance. The pressure cell has an inner diameter of 6.25 cm and a height of 17 cm. The pressure panel is a Trautwein pressure panel with 8 burettes; each consisting of an annulus and a pipette. Bentonite suspensions are freshly prepared and poured within 2 minutes into the pressure cell. The top of the pressure cell is connected to the pressure panel and the bottom to the permeameter. Bentonite suspensions of 6 to 11% concentration were injected into the sand permeameter at a constant pressure of 35kPa. An empty cup is placed on top of a balance to collect and measure weight of the effluent until no more effluent is expelled for a duration of 10 minutes. Figure 3-8 is a schematic diagram of the constant pressure permeation setup.

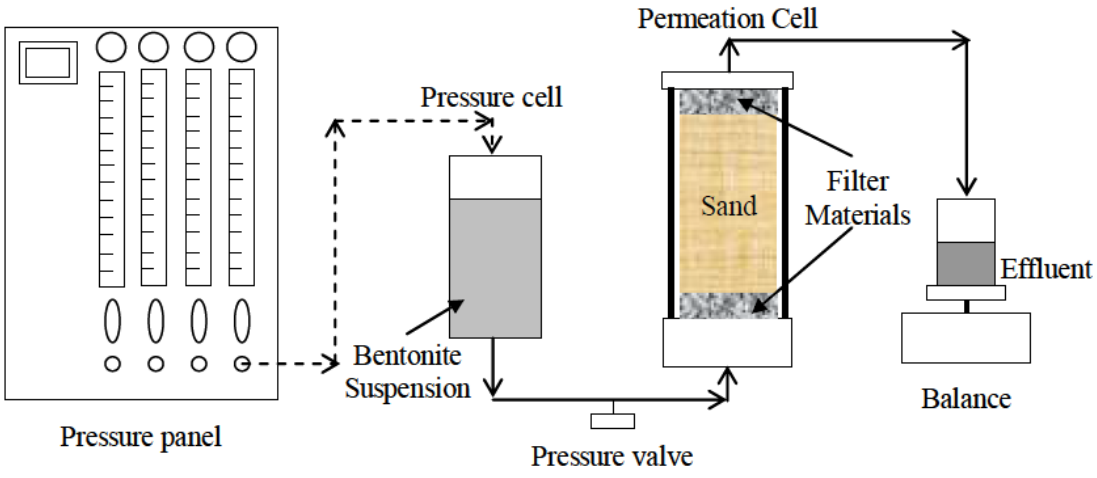

Figure 3-8: Schematic diagram of the constant pressure permeation setup (Adapted from Yoon, 2011)

3.3.3 Washing out setup

The hydraulic gradient at which bentonite suspensions are washed out from Sand permeated with bentonite suspensions was studied to evaluate the stability of trench or cutoff walls. Multiple hydraulic conductivity tests were performed at different hydraulic gradients to detect the degradation of bentonite suspensions.

Sample preparation

Sand permeated with bentonite suspensions samples were prepared for the washing out tests. The sample preparation setup consisted of 3 cylinders coupled together to form the permeameter. All 3 cylinders had an inner diameter of 7 cm; whereas, the top and bottom cylinders were 3.75 cm in height and the central cylinder was 5.1 cm in height. Two aluminum hose-clamps were used to ensure that the 3 cylinders are aligned. Each clamp was placed tightly at the joint between the bottom and middle permeameter or between middle and top permeameter. Two rubber liners were used in between the permeameters to ensure a perfect seal is maintained throughout the testing procedure. The aim of this setup is to provide uniform permeation of the sand with bentonite through the filter material. Also, if a bentonite cake is formed at the interface between the filter material and sand, it would not be included in the specimen used for the washout tests because the specimen would be obtained from the middle cylinder only. Figure 3-9 shows a picture of the assembled permeameter before and after sample preparation.

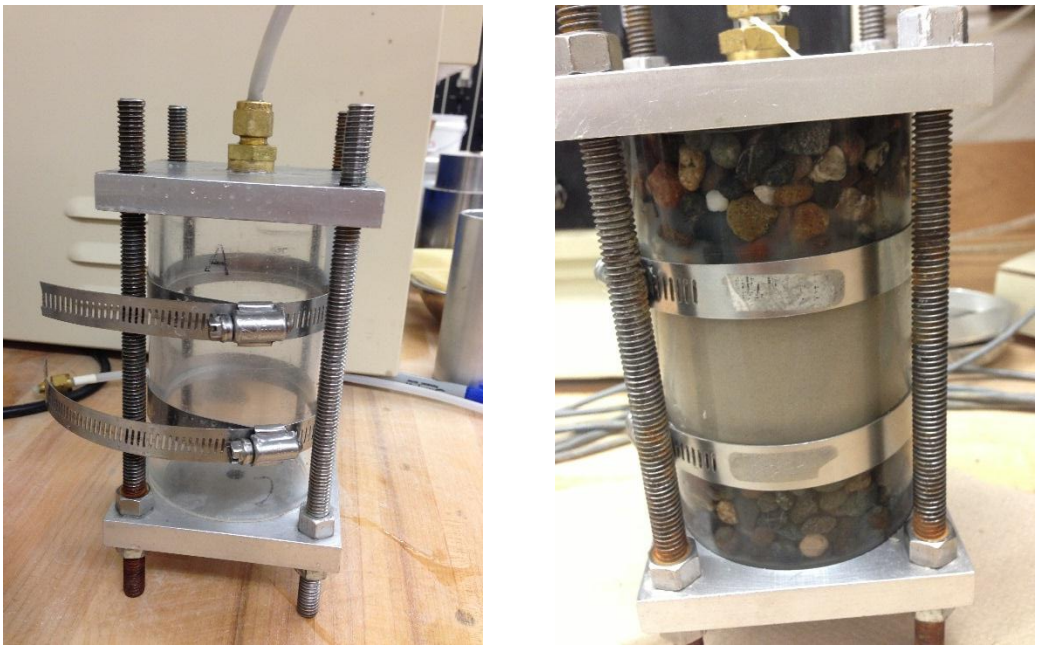

(a) (b)

Figure 3-9: (a) Permeation setup with 3 cylinders assembled, (b) permeation setup with permeated sample

Once the permeameter is set up, the sample is prepared in the same way as for the permeation setup. Filter material of thickness 2.5 cm are placed at the bottom and top of the sand and the sample is flushed with water for at least 3 times its pore volume. The specmens for washing out tests were permeated with bentonite under a constant flow rate to ensure uniform bentonite content in the sample. The constant flow tests were selected based on results by Yoon (2011) that showed such tests to provide a more uniform permeation than under constant pressure conditions due to reduced filtration. The reduced filtration implies that suspension in the voids has similar concentration as that before permeation and their properties (particularly yield stress) can be assumed to be equal to that of identical suspensions tested using the rheometer. The constant flow setup consists of a peristaltic pump manufactured by Stenner Pump Company (model 85MPH22), a pressure sensor manufactured by GEOTAC, injection line between pump and bentonite suspensions, and an injection line between the pump and the base of sample.

Bentonite suspensions were continuously mixed during the permeation process to prevent yield stress and viscosity build up. Figure 3-10 shows the constant flow permeation setup. After permeating the sample, it is left to rest for at least 24 hours or more depending on the yield stress to be tested during the washout tests. The permeameter is then disassembled and the top and bottom of the middle permeameter were cautiously trimmed with a wire saw to separate it from the top and bottom sections.

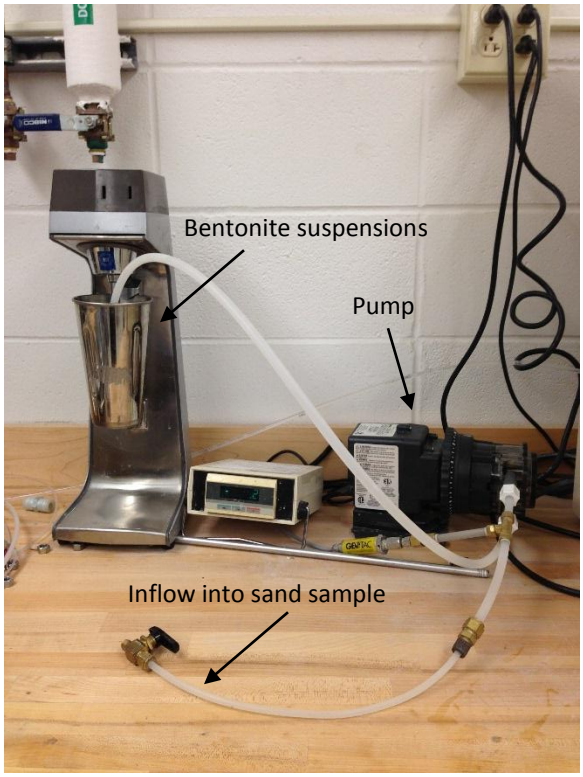

Figure 3-10: Constant flow setup

Hydraulic conductivity setup

Similar to the permeation setup, the 3 cylinders are assembled again using the rubber liners and coils. The bottom cylinder is filled with the pea gravel filter material and saturated with water. The trimmed middle permeameter of an inner diameter of 7 cm and a height of 5.1 cm is placed on top of the gravel with a filter paper in between. Filter paper with diameter 7.5 cm

is placed at the bottom of the sand permeated with bentonite suspensions to prevent sand or bentonite from seeping into the filter material. Afterwards, a mesh with a diameter of 6.5 cm and opening size of 0.043 cm is placed between the middle cylinder and the top one. The top cylinder is filled with pea gravel and saturated with water. The filter material are added at the top and bottom of the Sand permeated with bentonite suspensions to provide uniform flow through the cross sectional area of the sample. The sample is tightly closed with an air-tight plate.

As mentioned earlier, the washing out of bentonite suspensions from sand is detected by performing multiple modified hydraulic conductivity tests at various hydraulic gradients. All lines must be fully saturated with water before connecting them to the permeated sample. The bottom line is connected to the inflow burette of pressure panel; whereas, the top line is connected to the outflow burette. Figure 3-11 shows the modified hydraulic conductivity setup. The sample is connected to the pressure panel and is subjected to a back pressure of 300kPa to increase saturation. Back pressure was applied incrementally; 7 kPa was added every 3 minutes till 300 kPa was reached. The back pressure is then kept for 24 hours before a falling and rising head hydraulic conductivity test is conducted based on ASTM 5856-95 standards with gradients ranging from 0.2 to 25.

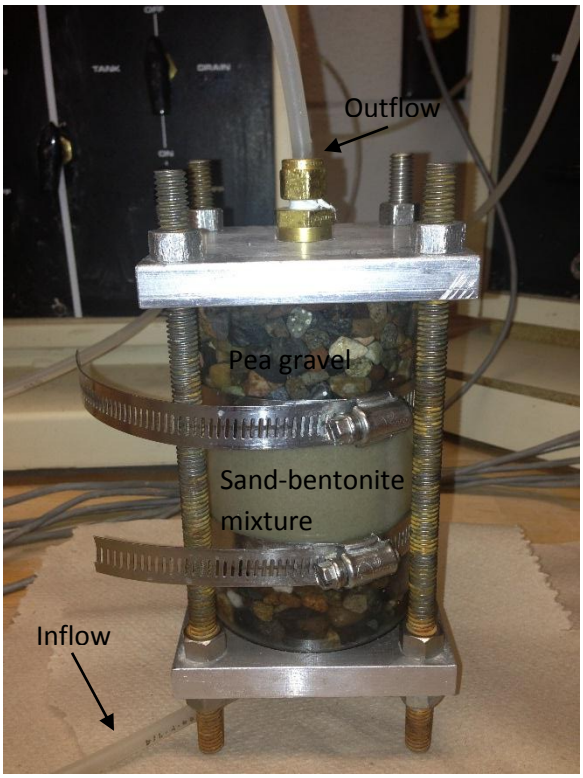

Figure 3-11: Modified hydraulic conductivity setup

During the hydraulic conductivity tests, inflow and outflow from the sample and the head difference were measured over time using differential transducers (Validyne Engineering, DP15) and the data required using a data acquisition system. The transducers along with the data acquisition system provide more accurate and reliable results than data collected by eye inspection, especially when the flow is slow. The pipettes are graded with a resolution up to 0.1ml, so it was difficult to detect little volume changes at low flow rates. The two pressure lines of the flow volume transducers are connected to the top and bottom of each pipette, and the volume of water flow is calculated based on the change in deferential pressure across the length of the burette. The head difference across the height of the specimen is measured as the differential pressure between the bottom of the outflow and inflow pipettes. The transducers had

to be calibrated to convert voltage to ml for flow measurements and psi for head difference measurements. The calibration method and calibration factors are discussed later on in this study.

Bentonite content

The bentonite content was measured at different locations in the specimen to better visualize the effect of washing out on Sand permeated with bentonite suspensions. Once the hydraulic conductivity tests were performed, the specimen was divided into 4 pieces: top left, top right, bottom left, and bottom right; using a wire saw and tested for bentonite content. Bentonite content was also measured at the core of the specimen. This was done by coring at the center of sample a diameter of 2.5 cm through the height of the specimen.

Bentonite content in Sand permeated with bentonite suspensions was measured using the wet sieving tests. Ottawa sand does not have fine and the bentonite was sieved through the No.200 sieve; therefore, the No.200 sieve was used to perform the wet sieving tests. The procedure is explained as follows:

1. Place the part of the specimen to be tested for bentonite content in an oven for 48 hours.
2. Weigh the dried sample while on the No.200 sieve.
3. Wash the sample with water through the No.200 sieve to remove the bentonite.
4. Dry the sand retained on the sieve in the oven for 48 hours.
5. Weigh the dried sand and the sieve.
6. Calculate the bentonite content from the weight of the dried sample before and after washing bentonite.

Pressure panel calibration

The differential pressure transducers (DPT) consist of a diaphragm placed between the transducer's plates. Based on the deformation of the diaphragm, an electric signal is sent to the computer through an interface car; UPC 2100 model. Since the diaphragm is very sensitive, it was crucial that the transducers lines connected to the bottom of the pipettes to be completely saturated, and the lines connected to the top of the pipettes to be clear of water. Also, the transducers were placed on a wooden wrack attached to the pressure panel to provide electrical isolation. The same sensor has a wide range of pressure capacities (ranges between ±0.08 psi and ±3200 psi) which can be controlled by the diaphragm placed within. The manufacturer Validyne provided 24 diaphragms with varying pressure. For outflow and inflow measurements, the No.26 diaphragm with pressure range ±0.5 psi was used. As for head difference measurements, the No.36 diaphragm with pressure range ±5 psi was used.

In this study, only 3 out of the 10 sensors were calibrated and used. Two sensors measured volume of water; whereas, one sensor measured head difference. The sensors were labeled to recognize the signal transmitted to the computer. Table 3-4 summarizes the sensors' label and position.

Table 3-4: Sensors' label and position

Sensor	Label	Measuring Variable	Unit
1	1A	Inflow	ml
2	2A	Pressure gradient	psi
3	3B	Outflow	ml

Sensors used to measure the volume of water in the pipettes were calibrated by increasing the volume of water at increments of 1 ml and recording the signal transmitted to the computer at

each increment. The signal was recorded for water volume ranging from 1 ml to 10 ml. The calibration factor is the linear correlation between the signal recorded and the eye detected volume. Similarly, the transducers used to measure head difference were calibrated by maintain the level of water constant in the one of pipettes and increasing the water level in the other by increments of 1 ml to reach 8 ml difference. 1 ml of volume of water was converted to pressure in psi whereby 1 ml is equivalent to 0.011 psi. The calibration factor is the linear correlation between the computer signal and the pressure based on volume reading. An offset factor was needed to finalize the calibration process. Note that the flow measurements were measured in ml and pressure difference in psi. Table 3-5 summarizes the calibration factors for each sensor.

Table 3-5: Sensors' calibration factor

Sensor	Calibration Factor
1	598.261462 (ml/V)
2	-18.333333 (psi/V)
3	249.735203 (ml/V)

The stability of the transducers' signal was measured to validate the accuracy of the test results. Each transducer was checked by filling the pipettes to 5 ml, applying a back pressure of 303 kPa and recording the signal for 24 hours at an interval 0.5 seconds. No specimen was connected to the pressure panel. Figure 3-12 show the signal check for sensors 1 (1A) and 2 (2A). For sensor 1, the signal varied between 4.93 and 5.03 with a ±1% error. As for sensor 2, the signal varied between 0.028 and 0.03 indicating static signal from the transducer.

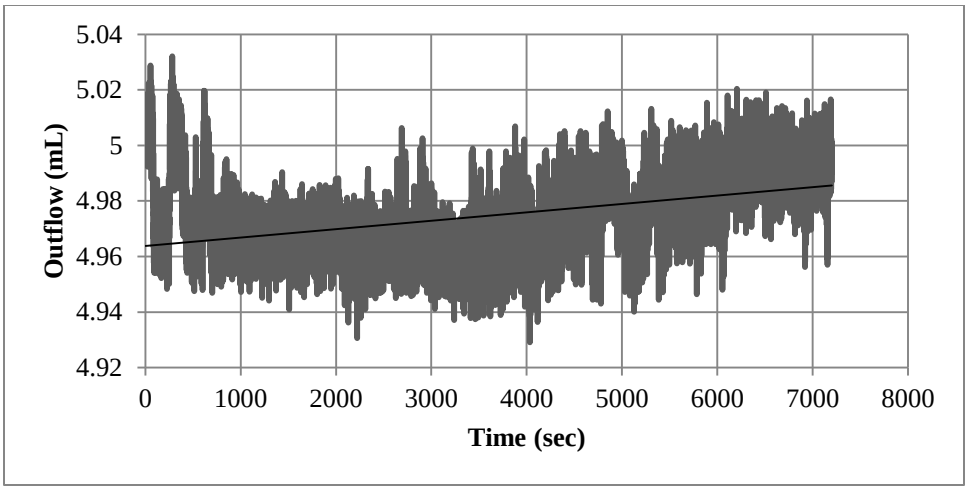

(a)

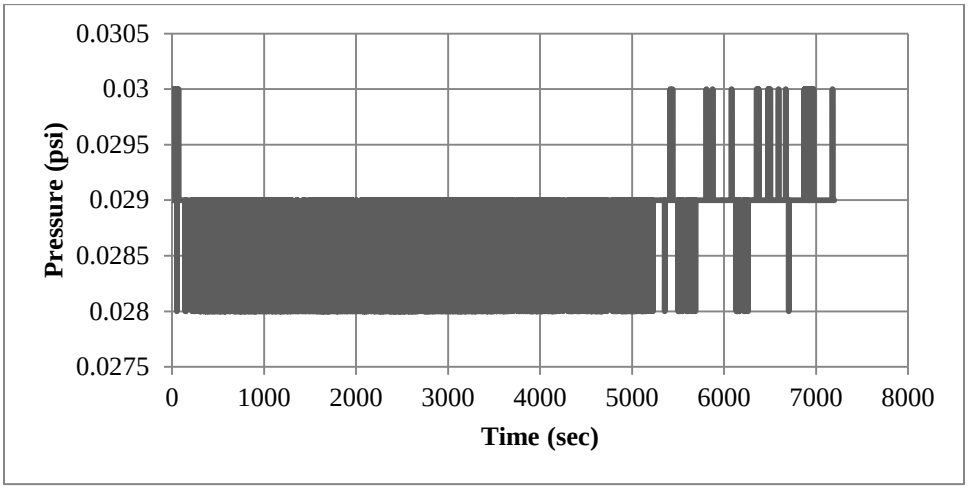

(b)

Figure 3-12: Signal check for (a) Sensor 1 1A, (b) Sensor 2 2A

3.4 Conclusions

The materials used during this study include sand, bentonite, water, and filter materials. All of the materials were characterized and described. The properties of bentonite were scrutinized because they affect the permeation and washing out test results. The properties included particle size, mineral composition, Atterberg limits, activity, pH, specific gravity, and specific area. The electric conductivity of tap, pure, and deionized water was measured, but only

deionized water was considered for this study. As for the filter materials, pea gravel and coarse sand was used to distribute the flow of water or bentonite uniformly across the sand sample.

The rheological, permeation, and washing out setups were described in details. The rheometer, device initialization, testing program, sample preparation, and storage process are presented for the rheological setup. The sample preparation procedure, permeation, and hydraulic conductivity tests are explained for the permeation setup and the washing out setup.

CHAPTER 4: RESULTS

4.1 Introduction

This chapter presents the results of the rheological experiments conducted on the unmodified and SPP modified bentonite suspensions, the permeation experiments performed with the four permeameters, and the washing out experiments. The rheology section summarizes the rheological properties of unmodified and modified bentonite suspensions over time. The permeation section includes the measured and calculated penetration depth of bentonite suspensions into sand at a pressure of 35 kPa in four permeameters with varying diameter size. As for the bentonite washing out section, the results of the hydraulic conductivity tests performed on sand permeated with bentonite suspensions are presented.

4.2 Rheology

The rheological properties of the unmodified and sodium pyrophosphate modified bentonite suspensions tested using the vane geometry described earlier are presented in this section. The properties tested include yield stress, apparent viscosity, phase angle, critical storage modulus, and critical strain. These properties were selected because they provide information on the strength of the flocculated structures and the transition from the liquid like to solid like behavior. During permeation grouting, the bentonite suspensions must have a very low viscosity for initial mobility to occur. However, it is also necessary that the viscosity increases rapidly to stop the flow and secure the stability of these suspensions in the soil. Therefore, the rheological properties of various fractions of unmodified and SPP modified bentonite suspension are studied at the initial time and with time. Bentonite fractions of 6, 7, 8, 9, and 10% were tested to evaluate the performance of unmodified suspensions; whereas bentonite fractions of 10, 11, and 12, with

SPP concentration of 1 to 3% were tested for the performance of modified suspensions. The time dependent behavior of modified and unmodified suspensions was studied at days 2, 5, 10, 15, and 20.

4.2.1 Initial flow behavior

The initial flow behavior of unmodified and SPP modified suspensions was determined to ensure that the suspensions have a mobility high enough to ensure adequate permeation grouting.

Yield Stress

The yield stress of unmodified and modified suspensions were determined immediately after mixing by conducting stress ramp tests on the rheometer setup. The yield stress increased exponentially as the bentonite fraction increased. Bentonite suspensions with bentonite fraction of 6% or less have a yield stress of zero at initial conditions. Figure 4-1 and Figure 4-2 show the relation between yield stress and bentonite fraction for unmodified and modified suspensions respectively. The yield stress increases as the bentonite fractions increases; whereas, the yield stress decreases as the concentration of SPP increases.

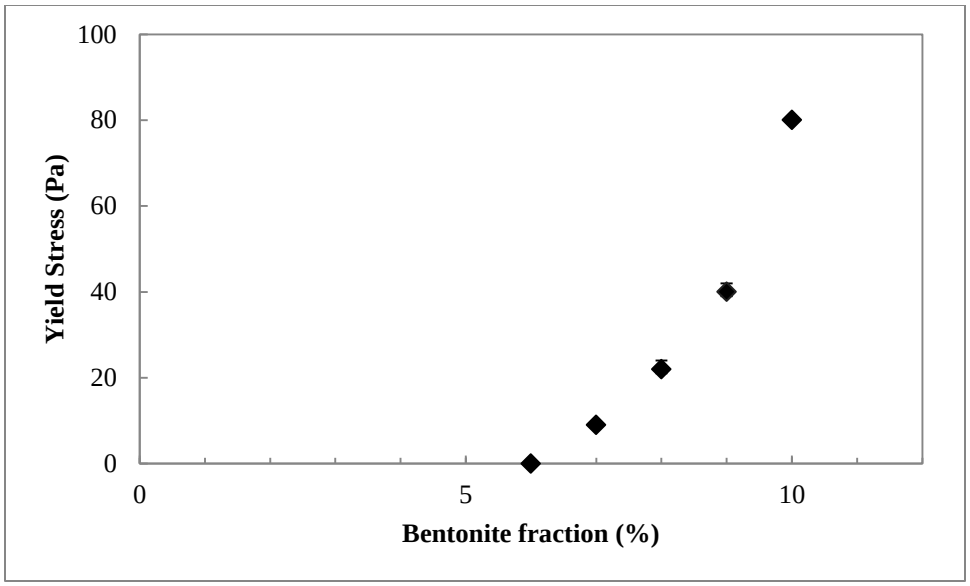

Figure 4-1: Yield Stress versus bentonite fraction for unmodified suspensions

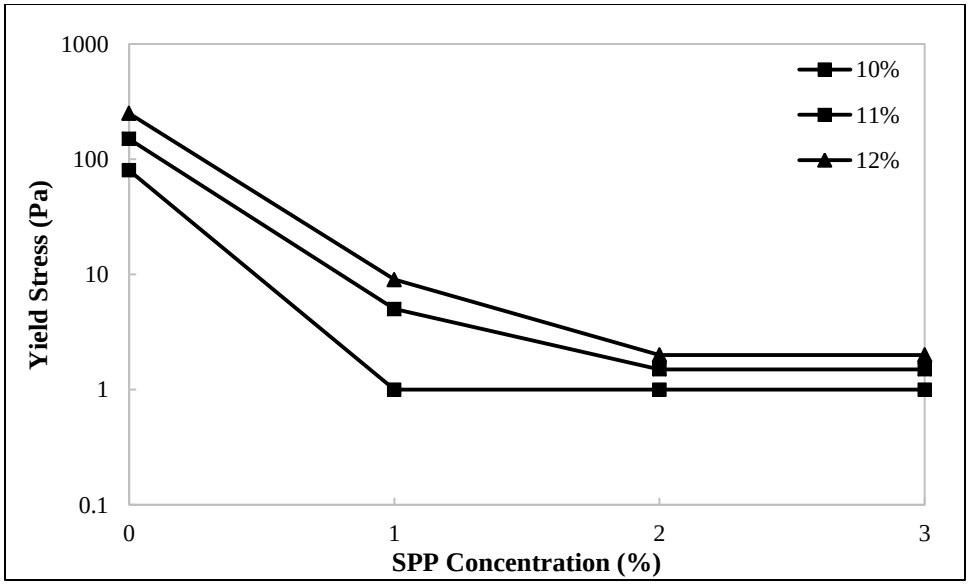

Figure 4-2: Yield stress versus bentonite fraction for modified suspensions

Apparent viscosity

The viscosity of bentonite suspensions is shear rate dependent. For a certain bentonite fraction, the viscosity decreases exponentially as the shear rate increases. For this study, the viscosity at a shear rate of 200 s^{-1} is of interest and defined as equilibrium viscosity. Figure 4-3 is a plot of the apparent viscosity at a shear rate of 200 s^{-1} for bentonite fractions of 6 to 10%;

whereas, Figure 4-4 is the apparent viscosity for modified bentonite suspensions of fractions of 10 to 12% and SPP concentration of 0 to 3%. The apparent viscosity increased as the bentonite fraction increased; however, it decreased as the concentration of SPP increased.

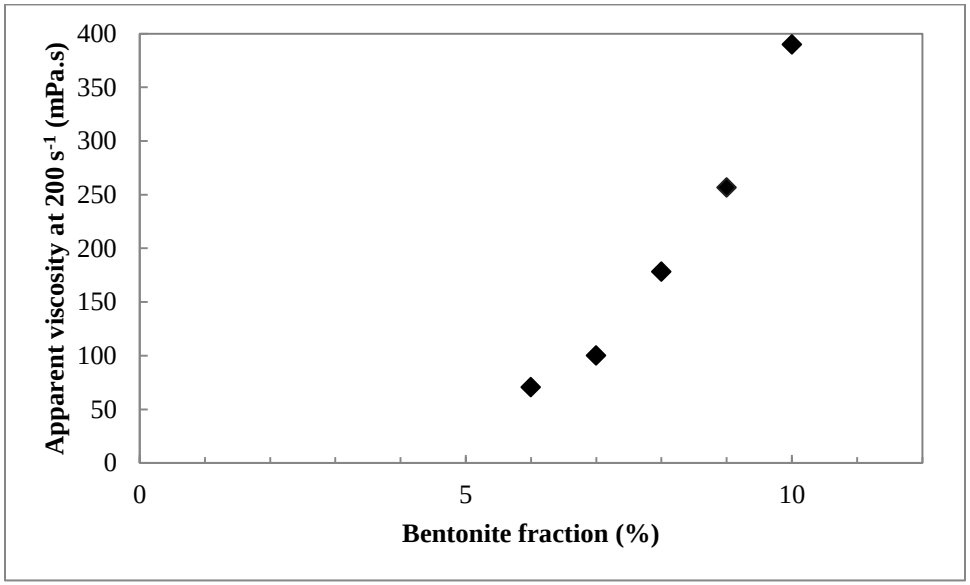

Figure 4-3: Viscosity versus bentonite fraction for unmodified suspensions

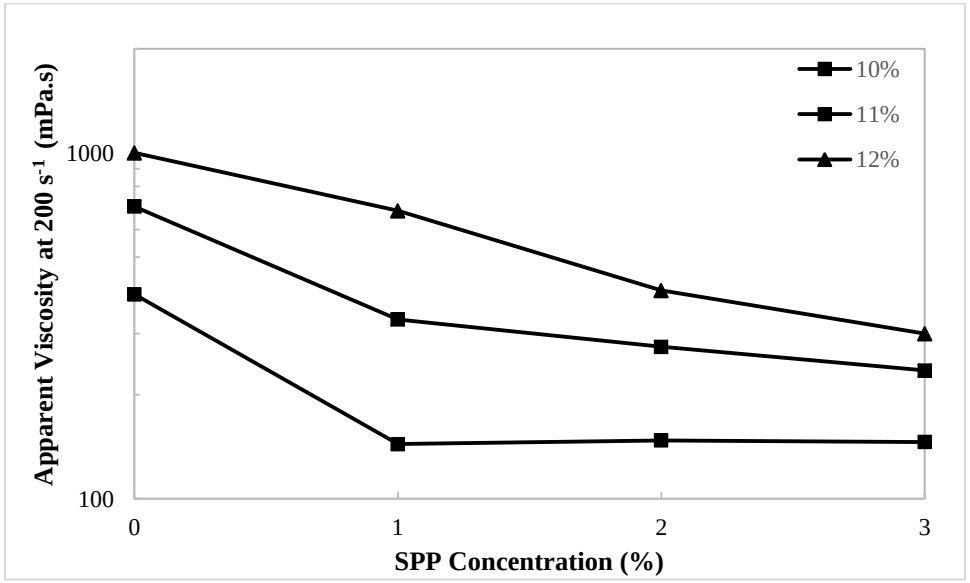

Figure 4-4: Viscosity at a shear rate of 200 s^{-1} for modified suspensions

Phase angle, critical strain, and critical storage modulus

Strain sweep tests were performed on different concentrations of unmodified and SPP modified bentonite suspensions to determine the phase angle, critical strain, and critical storage modulus. The critical storage modulus and critical strain were determined using the procedure described in Chapter 3 and plotted in Figure 3-4. The critical modulus increases and the critical strain decreases as the bentonite fraction increases as shown in Figure 4-5. Figure 4-6 shows the variation of the storage modulus with strain for bentonite fractions of 6 to 10%. At any given strain, the storage modulus is greater for higher bentonite fractions. For a given bentonite fraction, the modulus remains constant until the critical strain is exceeded and afterwards it decreases exponentially. At strains greater than the critical strain, the bentonite suspensions are transitioned from solid to liquid-like behavior due to the degradation of the microstructure. Similarly, the phase angle remains constant for strains less than the critical strain and then increases exponentially with larger strains (Figure 4-7). Although all bentonite suspensions displayed a solid-like behavior since the phase angle remained less than 45˚, the phase angle decreases as the bentonite fraction increases indicating that the more concentrated suspensions have more of a solid-like behavior.

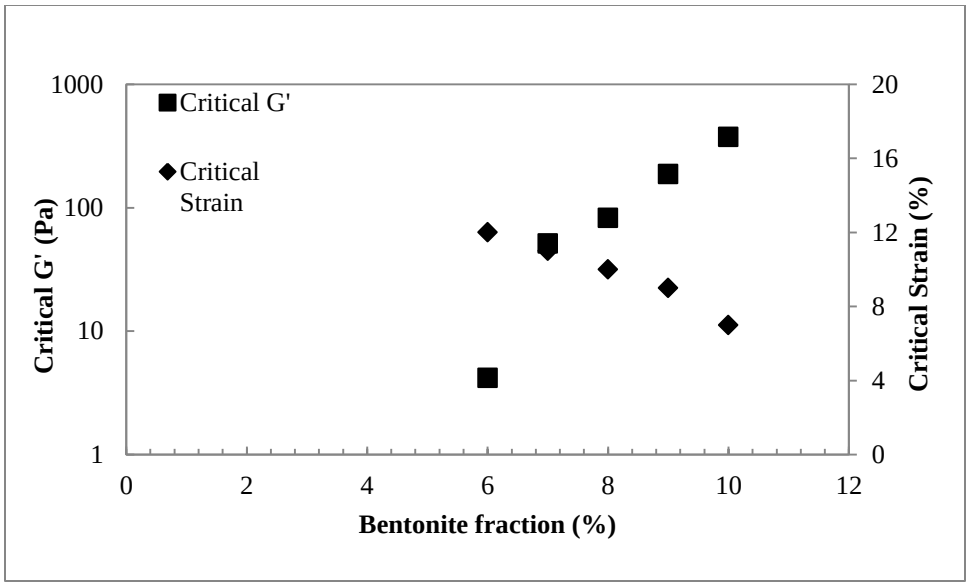

Figure 4-5: Critical G' and critical strain versus bentonite fraction

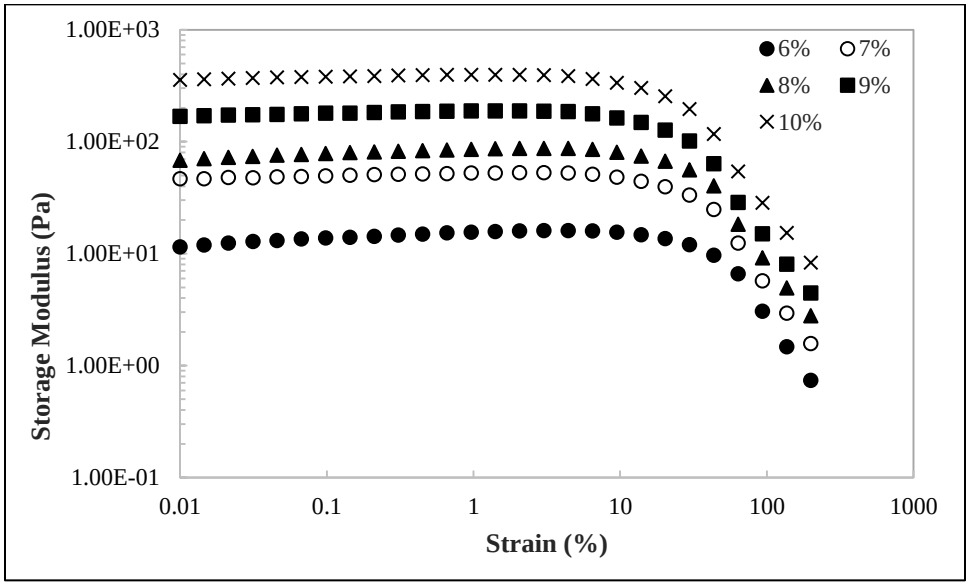

Figure 4-6: Storage modulus versus strain for unmodified bentonite suspensions

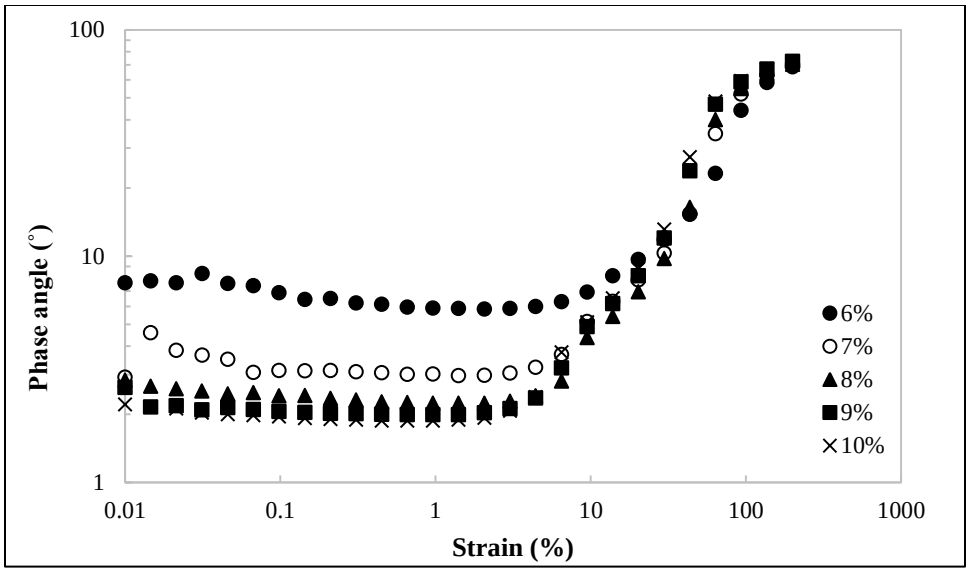

Figure 4-7: Phase angle versus strain for unmodified bentonite suspensions

The flocculated 3-D structure of the bentonite suspensions is affected by the addition of SPP. As the concentration of SPP increased for the same bentonite content, the critical storage modulus decreased and the critical strain slightly increased. The variation in the critical modulus and the critical strain converges with higher SPP concentration. Figure 4-8 plot critical modulus and critical strain for 10% and 11% bentonite fraction and increasing SPP concentration.

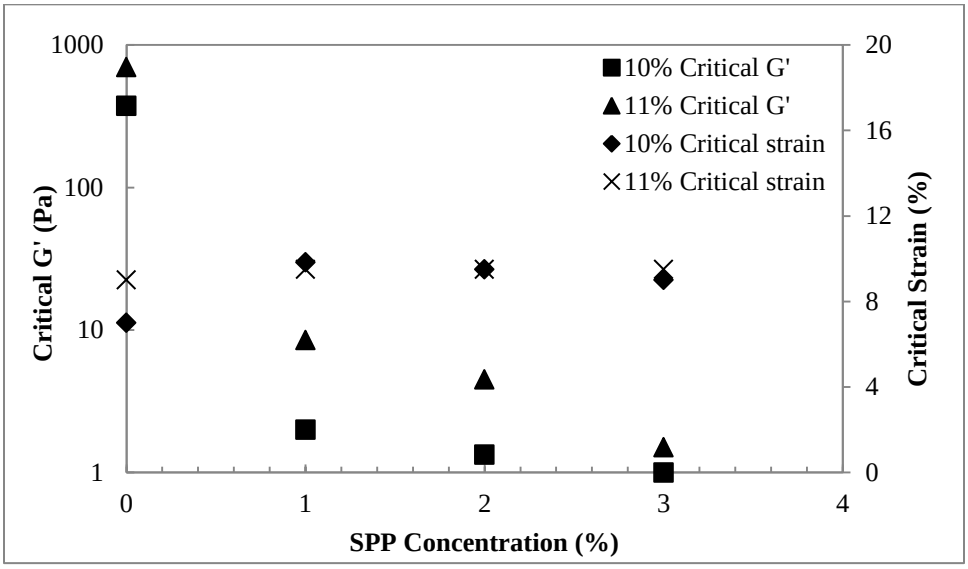

Figure 4-8: Critical G' and critical strain for bentonite fractions of 10% and 11% and SPP concentration from 0 to 3%

4.2.2 Time dependent behavior

The time dependent flow behavior of unmodified and SPP modified suspensions was determined to ensure that the mobility of the suspensions is reduced in time to ensure flow stoppage and stability in the grouted soil. The change in the properties of bentonite suspensions with time is more prominent in SPP modified suspensions. SPP does not alter the thixotropic nature of the bentonite suspensions. SPP reduces the yield stress and viscosity of the bentonite suspensions initially; however, strength is retained rapidly until it converges.

Yield Stress

The yield stress of unmodified and modified suspensions was determined at different resting times; day 2, day 5, day 10, day 15, and day 20. Figure 4-9 shows the variation of yield stress with time for unmodified suspensions of bentonite fraction 6 to 10%. The yield stress increased rapidly with time at first and then at a slower pace. At the same testing time, bentonite suspensions with greater bentonite fraction constantly had higher yield stresses.

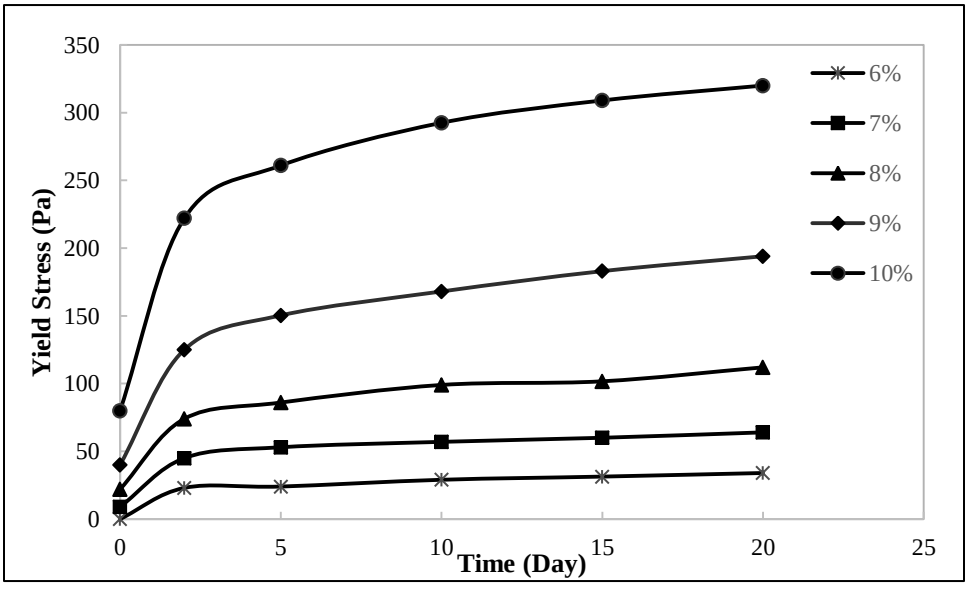

Figure 4-9: Variation of yield stress with time for bentonite fractions 6, 7, 8, 9, and 10%

The yield stress of SPP modified suspensions was also determined at different resting times. Figure 4-10 shows the variation of yield stress with time at different SPP concentrations for bentonite fraction of 11%. The addition of SPP caused the yield stress of the bentonite suspensions to decrease. As time passes, the yield stress increases rapidly until it converges to the yield stress of unmodified suspensions. For the same bentonite fraction, as the concentration of SPP increased, the initial yield stress decreased.

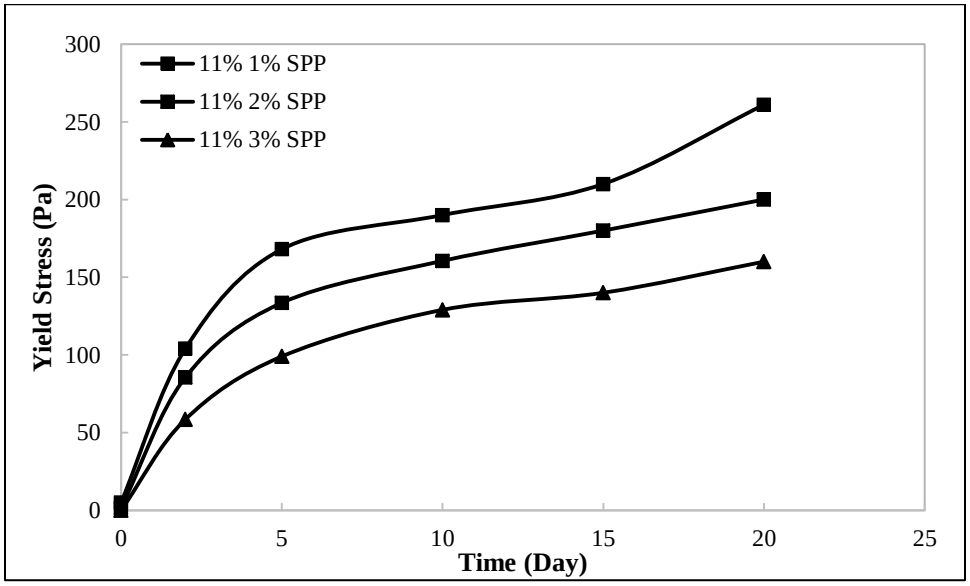

Figure 4-10: Variation of yield stress with time for bentonite fraction of 11% with 1, 2, and 3% SPP

The yield stress of bentonite suspensions with various bentonite fractions and SPP concentrations was determined to develop a relation between yield stress and post-grouting stability of sands permeated with bentonite suspensions. The bentonite suspensions had bentonite fractions varying between 13 and 16% and SPP concentrations of 3, 5, 7, 11, and 14%. Figure 4-11 shows the yield stress of the bentonite suspensions tested at different times.

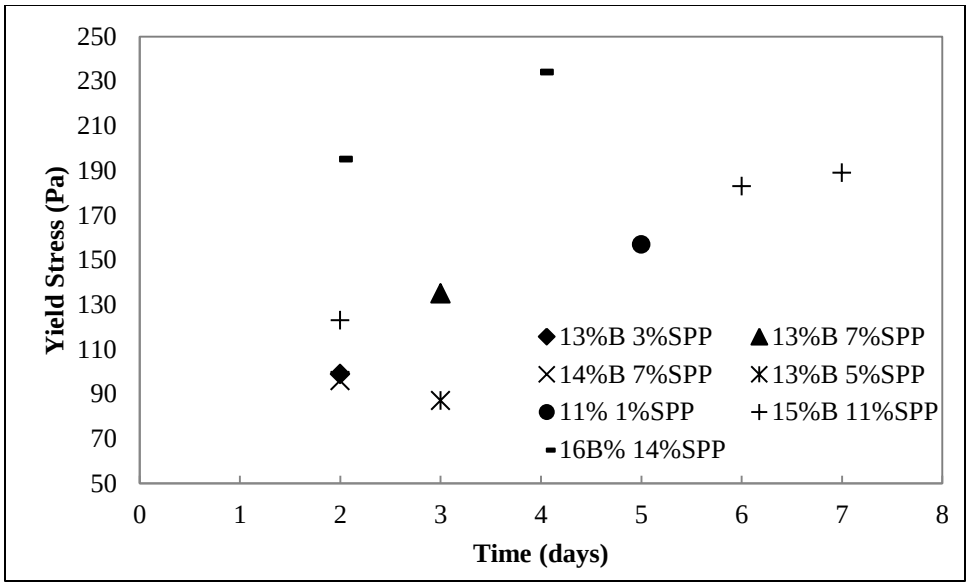

Figure 4-11: Yield stress of bentonite suspensions tested for washing out

Apparent viscosity

The apparent viscosity of modified and unmodified bentonite suspensions was determined with time. Figure 4-12 shows the apparent viscosity at a shear rate of 200 s^{-} for unmodified suspensions with bentonite fractions of 6, 7, 8, 9, and 10%. For bentonite fractions of 6, 7, and 8%, the equilibrium viscosity increased rapidly at first and then increased slightly with time. However, the equilibrium viscosity of bentonite suspensions with higher bentonite fractions continued to increase rapidly over time. Figure 4-13 indicates the variation of apparent viscosity at a shear rate of 200 s^{-1} for bentonite fractions of 10% with 0, 1, and 2% SPP over time. The apparent viscosity increased with time for bentonite suspensions with and without SPP; however, modified bentonite suspensions did not recover the viscosity of those unmodified.

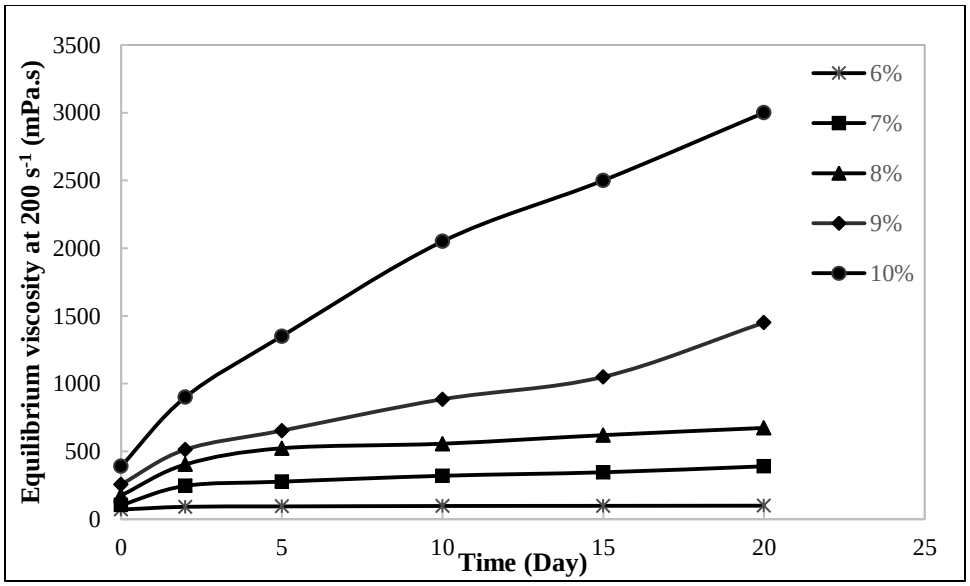

Figure 4-12: Variation of the equilibrium viscosity at a shear rate of 200 s^{-1} with time for bentonite fractions of 6, 7, 8, 9, and 10%

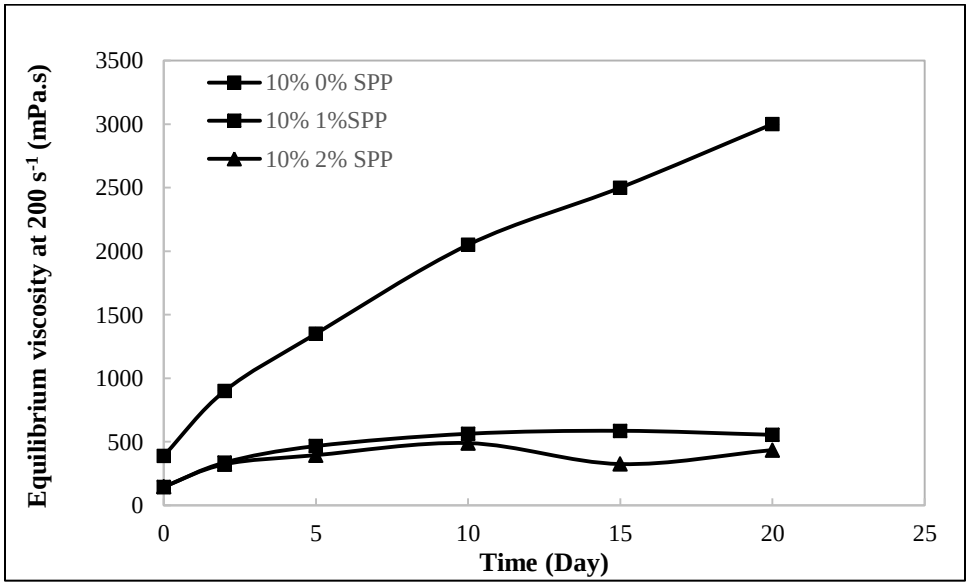

Figure 4-13: Variation of the equilibrium viscosity at a shear rate of 200 s-1 with time for bentonite fractions of 10% with 0, 1, and 2% SPP

Phase angle, critical strain, and critical storage modulus

The phase angle, critical strain, and critical storage modulus for modified and unmodified bentonite suspensions were determined at different times. Similar to the yield stress, the critical storage modulus increased with time. Figure 4-14 shows the variation of critical storage modulus with time for unmodified suspensions of 6, 7, 8, 9, and 10%. For all bentonite fractions, the

critical storage modulus increased with time, particularly at first. At all times, bentonite suspensions with greater bentonite fractions had a greater critical storage modulus. Figure 4-15 shows the variation of the critical storage modulus and critical strain with time for 10% bentonite suspensions with 0, 1, and 2% SPP. The storage modulus increased with time for both modified and unmodified bentonite suspensions, but the increase is less rapid with modified suspensions and the unmodified critical storage modulus was not recovered. As for the critical strain, it remained constant with time for both modified and unmodified suspensions except at initial mixing time for the unmodified suspensions.

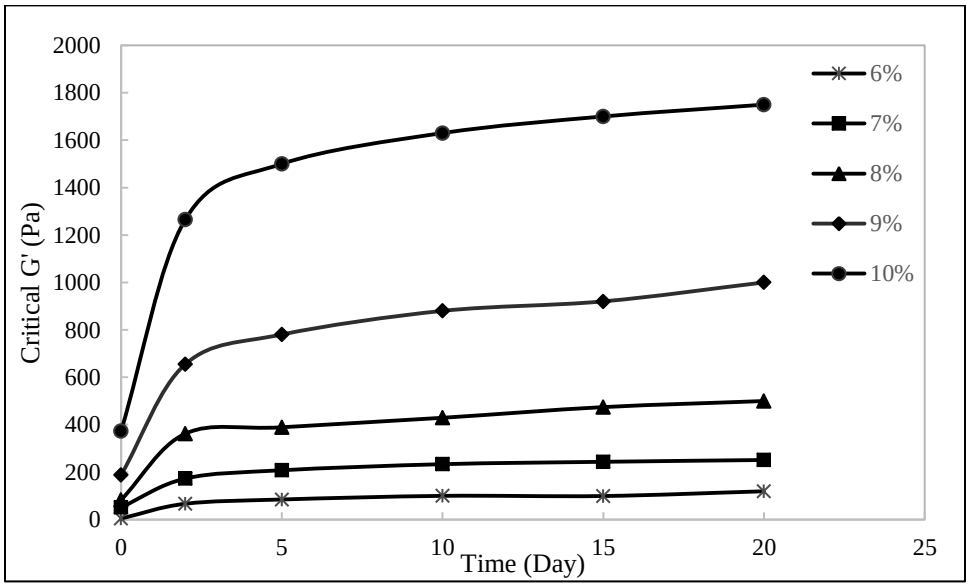

Figure 4-14: Variation of critical G' with time for bentonite fractions of 6, 7, 8, 9, and 10%

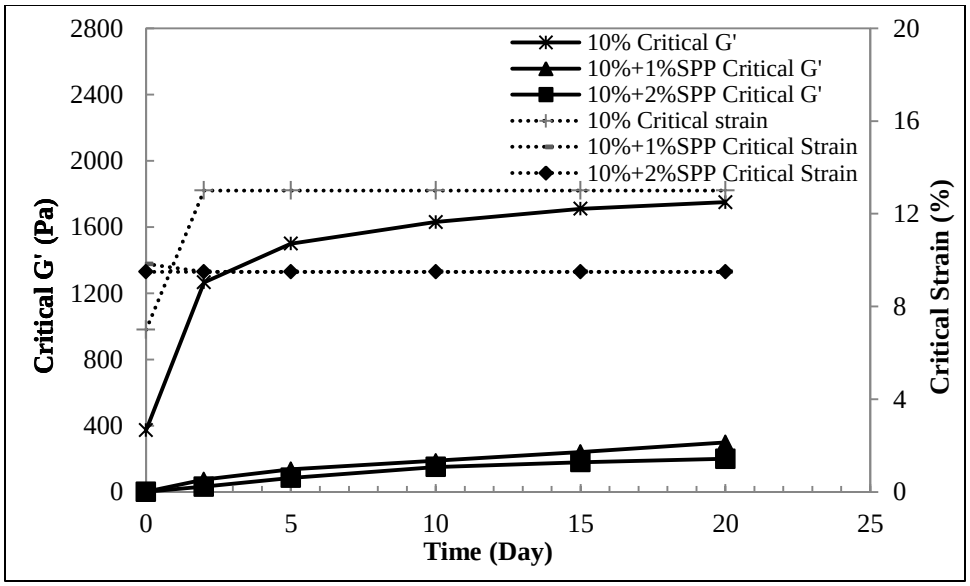

Figure 4-15: Variation of critical G' and critical strain with time for 10% bentonite fraction with 0, 1 and 2% SPP

Figure 4-16 and Figure 4-17 show the variation of the phase angle versus strain over time for bentonite suspensions of 9% bentonite fraction and 11% bentonite fraction with 1% SPP, respectively. For the unmodified suspensions, the phase angle slightly decreased with time especially between initial mixing time and day 2. As for the modified bentonite suspensions, the phase angle decreased more evidently with time which is expected since the bentonite suspensions become stronger as time passes and behave more like a gel. However, the phase angle experienced less variation at higher strains for both unmodified and modified bentonite suspensions.

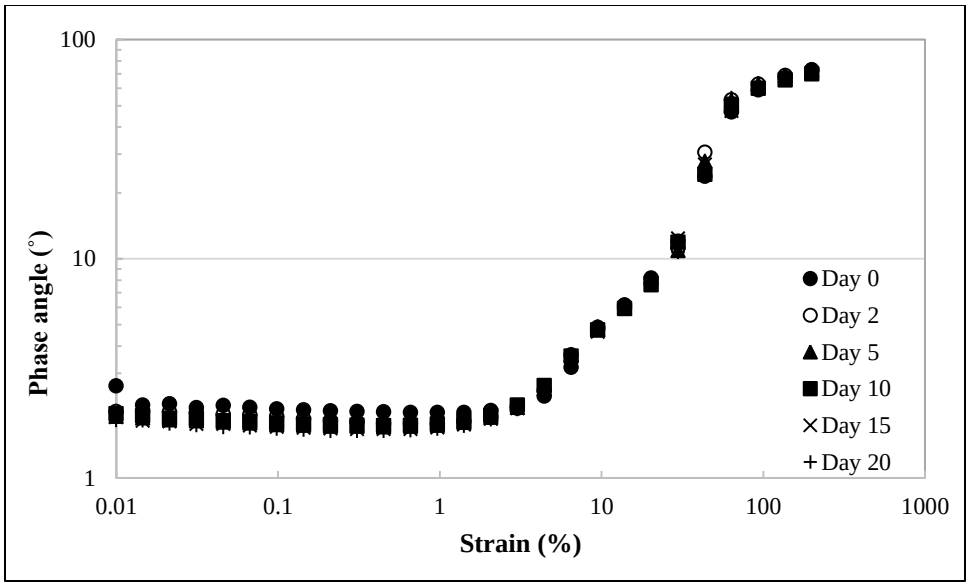

Figure 4-16: Variation of phase angle versus strain over time for bentonite suspensions of 9% bentonite fraction

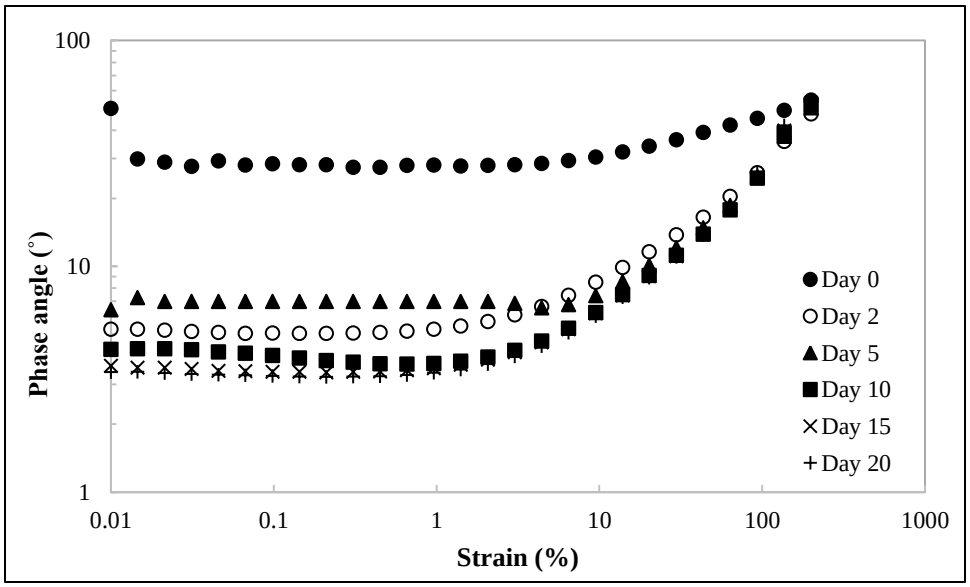

Figure 4-17: Variation of phase angle versus strain over time for bentonite suspensions of 11% bentonite fraction and 1% SPP

4.3 Permeation

The results of penetrability of bentonite suspensions through sand is presented in this section. Penetrability is the permeation distance the suspensions can travel during injection under a predetermined maximum pressure (Santagata and Santagata, 2003). The constant pressure technique used in this study gives insight on the effect of the soil, grout, and experimental

parameters on the grout flow; however, it is not reflect the in-situ multistage injection (Santagata and Santagata, 2003). The penetration distance of bentonite suspensions into sand was estimated by eye inspection and calculation. The volume of injection suspensions was used to calculate the penetration distance based on the area of the permeameter and porosity of sand. The volume was measured by weighing the water effluent and assuming it is equal to the volume of suspensions injected.

Yoon (2011) estimated an empirical equation that estimates the penetration distance of bentonite suspensions into sand based on equilibrium viscosity and grout and soil grain size. The equation was developed based on penetrability results for a permeameter of diameter 3.8 cm. In this study, the penetration distance was investigated for permeameters of diameter 3.8, 7, 10, and 14 cm. Figure 4-18 shows the penetration distance observed for various equilibrium viscosities (bentonite suspensions of bentonite fractions 6, 7.5, 8 9, 10, and 11%) for all permeameter sizes studied at 35 kPa. Also, the observed penetration distances versus permeameter diameter for bentonite fractions 7.5 and 10% are plotted in Figure 4-19. The permeameters with diameters of 7 cm or greater resulted in equal penetration distances for the same equilibrium viscosity. However, the penetration distance was greater for the 3.8 cm diameter permeameter. The penetration distance for the larger permeameter were adjusted to match the trend line for the 3.8 cm permeameter. A common calibration factor of 0.41 was used to adjust the results. Figure 4-20 shows the adjusted penetration distance for all permeameters and the trend line for the 3.8 cm permeameter at 35 kPa.

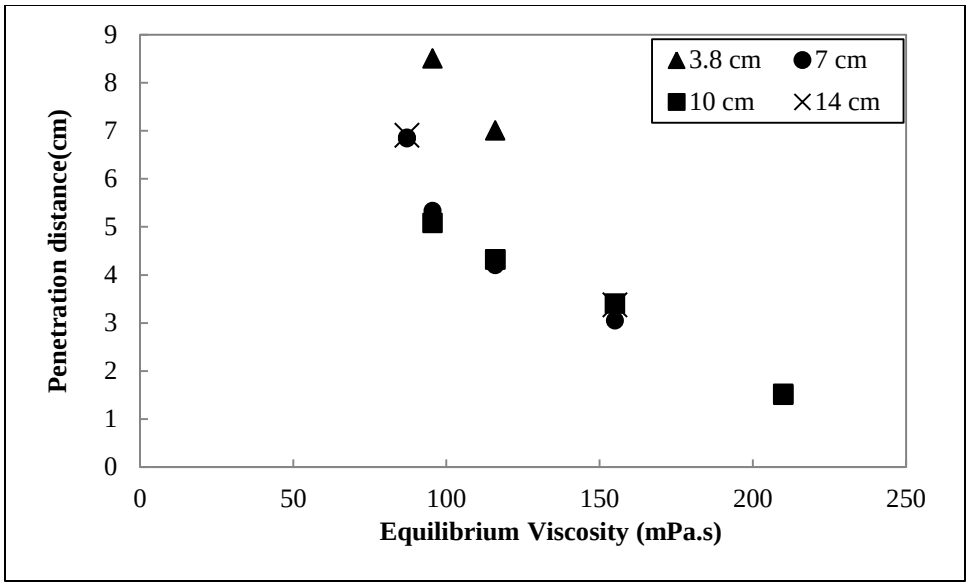

Figure 4-18: Observed penetration distance for multiple bentonite fractions

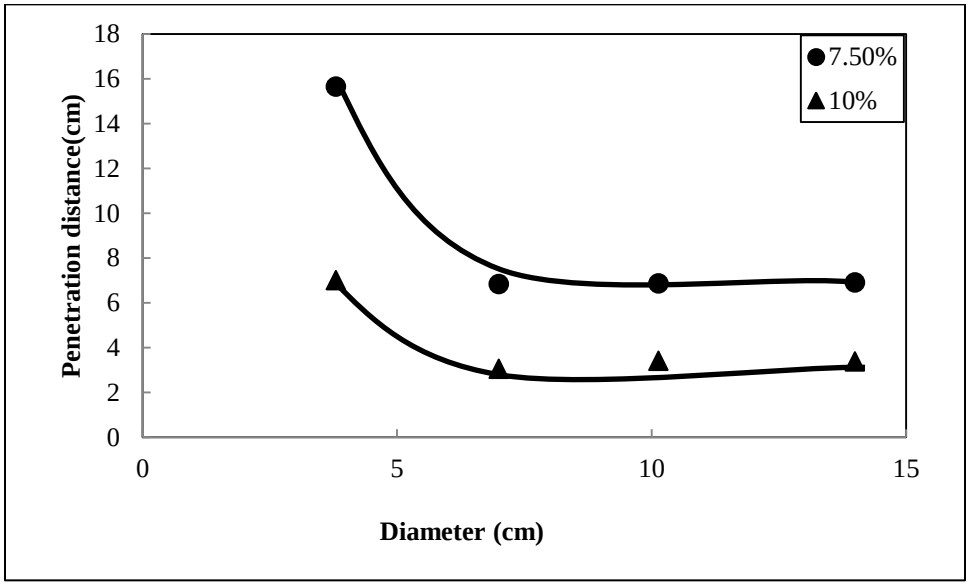

Figure 4-19: Observed penetration distance versus diameter of permeameter

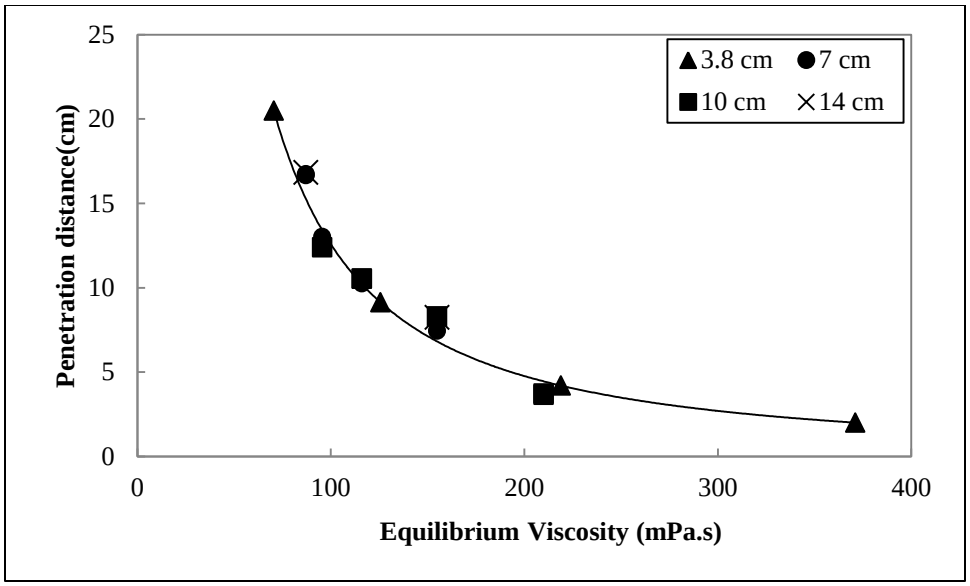

Figure 4-20: Adjusted penetration distance versus equilibrium viscosity

4.4 Bentonite Washing out

The purpose of the sand permeated with bentonite suspensions is to have a hydraulic conductivity low enough to form a hydraulic barrier and hence reducing under seepage. Once the hydraulic barrier is built, its stability under high hydraulic gradients becomes key. The stability and the hydraulic performance of sand permeated with bentonite suspensions was evaluated and the results are presented in this chapter.

4.4.1 Threshhold bentonite content

The hydraulic conductivity of the sand permeated with bentonite suspensions depends on the bentonite content (weight of bentonite/weight of sand). Figure 4-21 shows the variation of the hydraulic conductivity versus bentonite content. For bentonite content less than 3%, water flows through pores in the sand matrix that are not fully blocked with bentonite suspensions. Therefore, the hydraulic conductivity is that of clean sand or a reduced percentage of it. However, for bentonite contents greater than 3%, the hydraulic conductivity is significantly reduced because sand pores are fully grouted and water flows the clay voids.

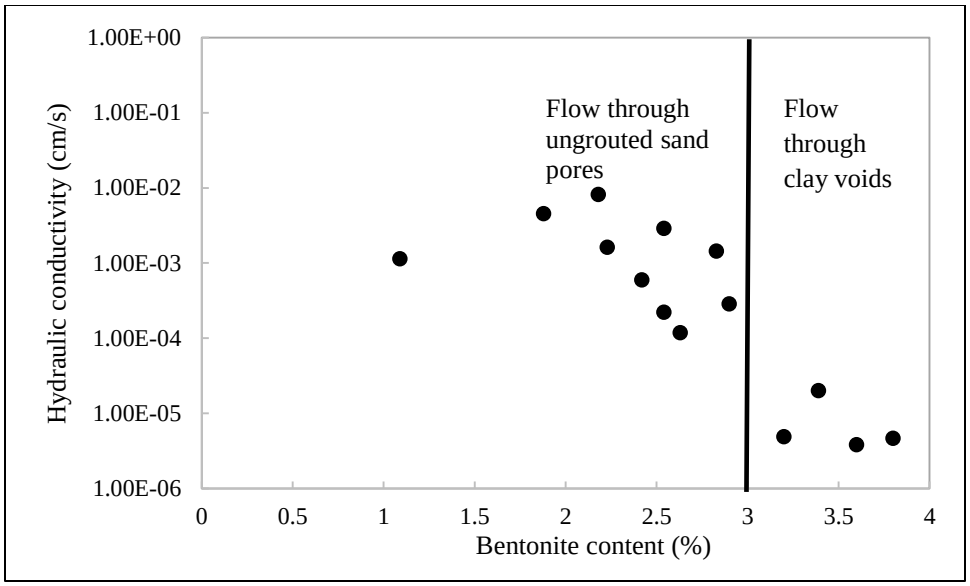

Figure 4-21: Hydraulic conductivity versus bentonite content

4.4.2 Post-grouting stability tests

The post-grouting stability of sand permeated with bentonite suspensions was tested by performing multiple hydraulic conductivity tests with increasing (forward) and decreasing (backwards) hydraulic gradients. The stability of the permeated sand was monitored by measuring its hydraulic conductivity at the different gradients. Figures 4-22 to 4-27 show the variation of hydraulic conductivity versus hydraulic gradient for bentonite suspensions with 13% bentonite fraction and 3% SPP, 13% bentonite fraction and 5% SPP, 13% bentonite fraction and 7% SPP, 14% bentonite fraction and 7% SPP, 15% bentonite fraction and 11% SPP, and 16% bentonite fraction and 14% SPP; respectively.

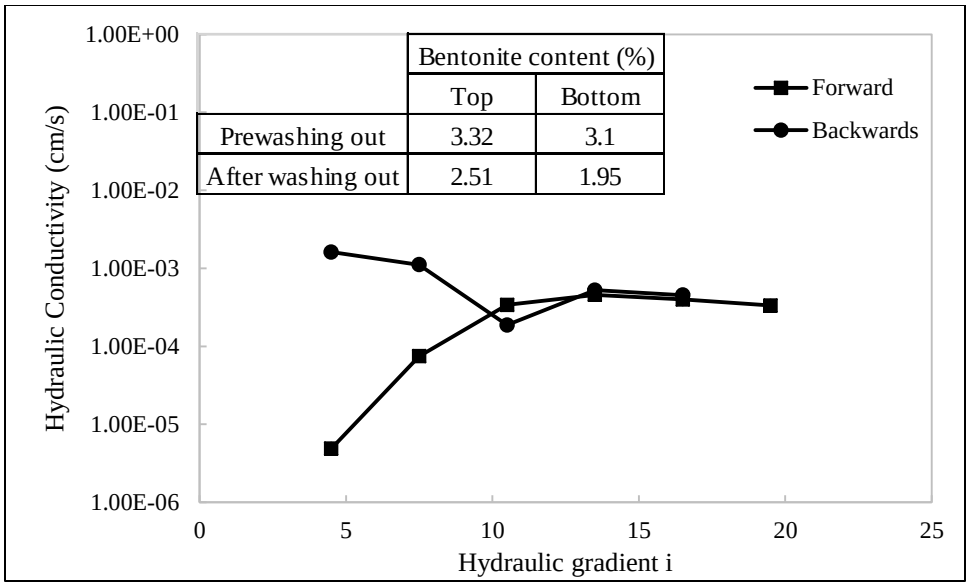

Figure 4-22: Hydraulic conductivity versus hydraulic gradient for 13% bentonite fraction and 3% SPP

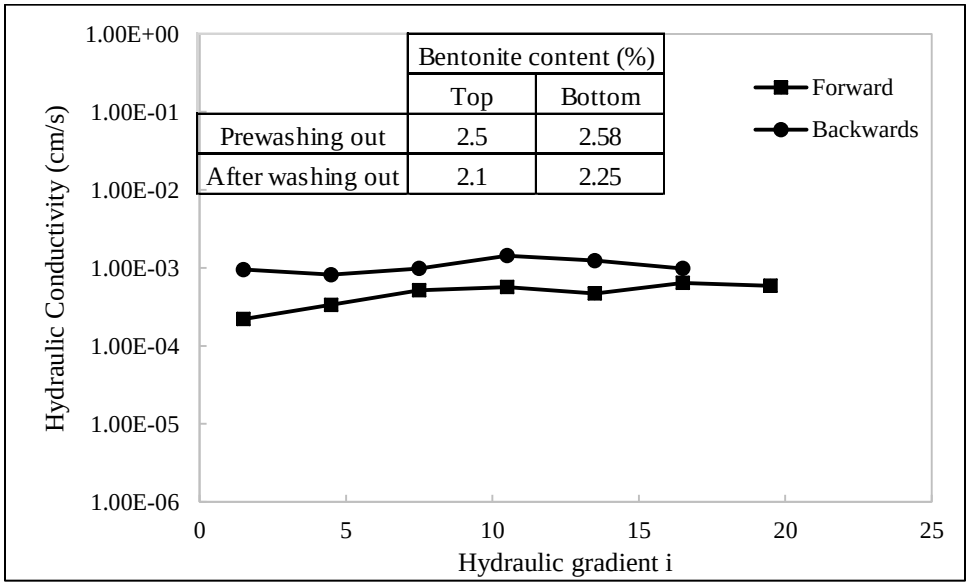

Figure 4-23: Hydraulic conductivity versus hydraulic gradient for 13% bentonite fraction and 5% SPP

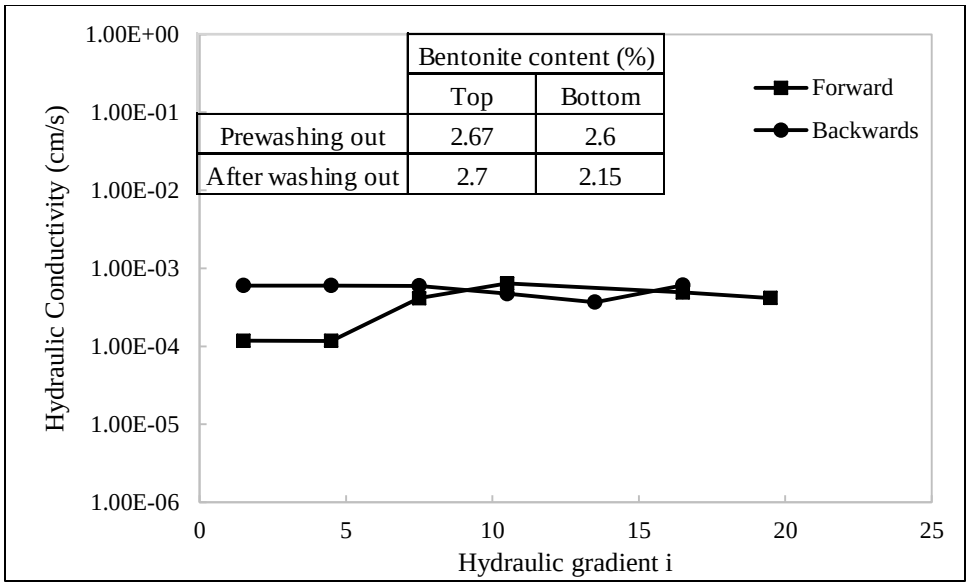

Figure 4-24 : Hydraulic conductivity versus hydraulic gradient for 13% bentonite fraction and 7% SPP

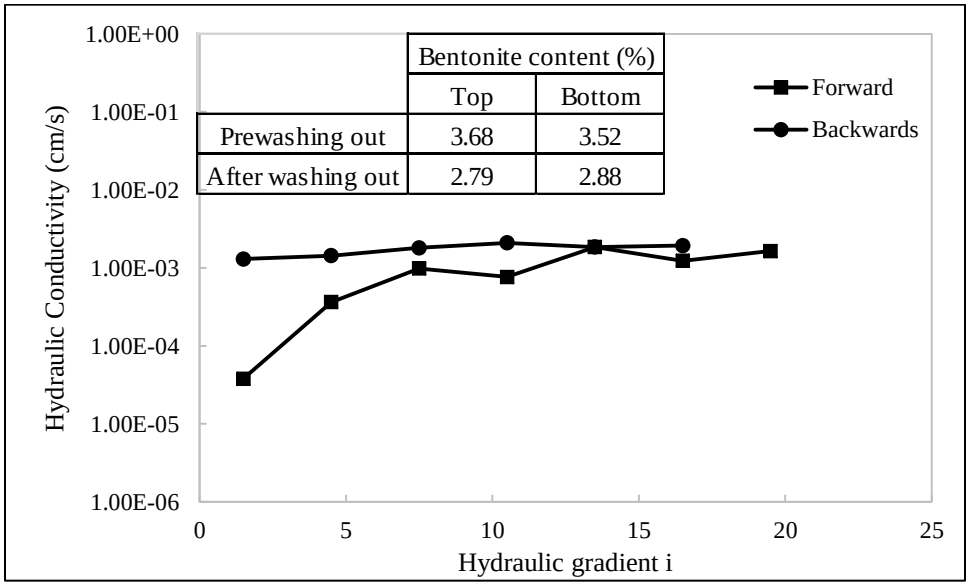

Figure 4-25: Hydraulic conductivity versus hydraulic gradient for 14% bentonite fraction and 7% SPP

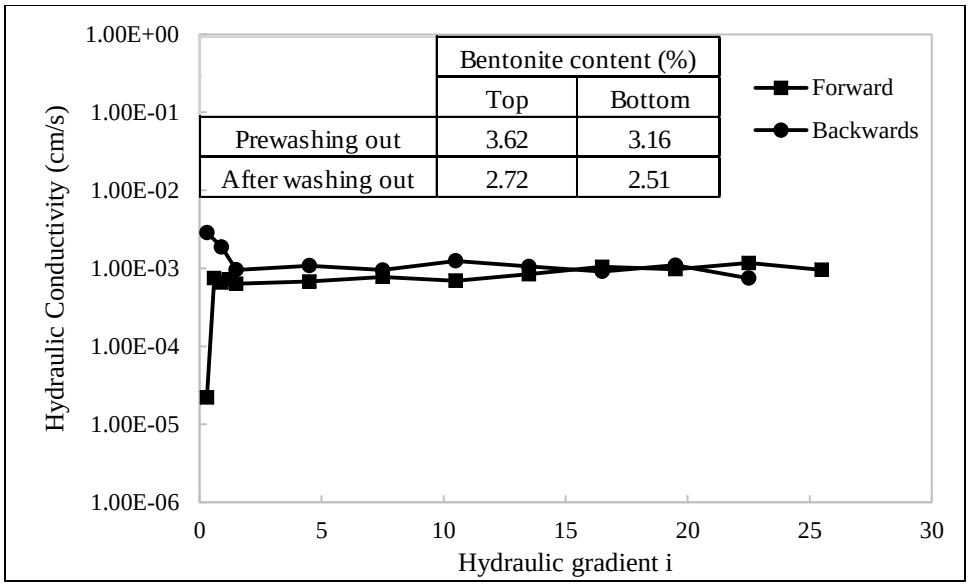

Figure 4-26: Hydraulic conductivity versus hydraulic gradient for 15% bentonite fraction and 11% SPP

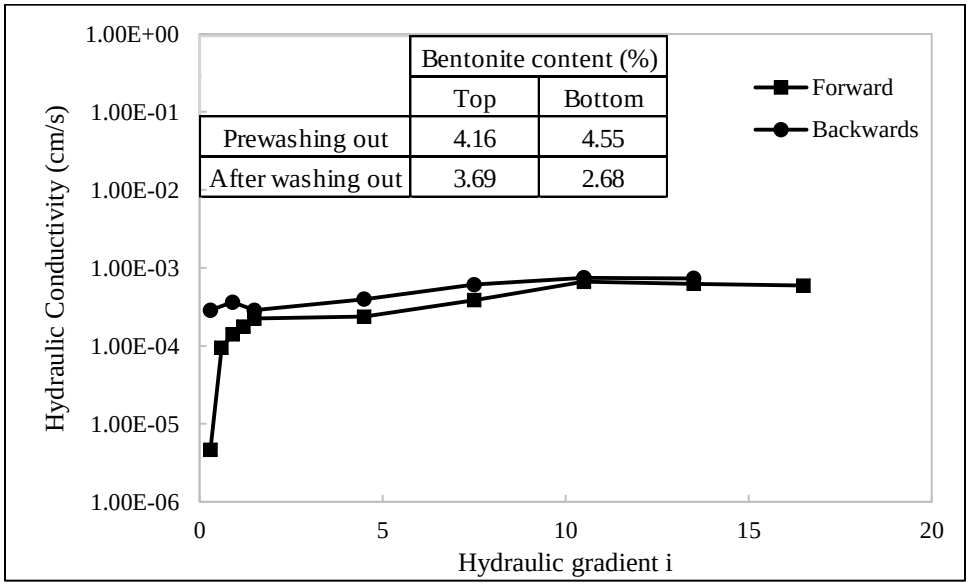

Figure 4-27: Hydraulic conductivity versus hydraulic gradient for 16% bentonite fraction and 14% SPP

4.5 Conclusions

The rheological properties of unmodified and modified bentonite suspensions were studied using the vane geometry. Bentonite suspensions with bentonite fractions varying from 7.5 to 12% and SPP concentration of 0 to 3% were investigated straight after mixing and over time. The yield stress, equilibrium viscosity, storage modulus, and loss modulus increased with

increasing bentonite fraction and over time. However, for the same bentonite fraction, the yield stress, equilibrium viscosity, storage modulus, and loss modulus decreased with increasing SPP concentrations. The reduced yield stress and apparent viscosity was recovered with time at an exponential rate. In addition, the yield stress of bentonite suspensions of fraction 13 to 16% and SPP concentration of 3 to 14% was determined to study the effect of yield stress of washing out.

Yoon, 2011 developed an equation that predicts the penetration depth of bentonite suspensions into sand. A series of injection tests using the constant pressure technique were performed to test the effect of the permeameter diameter size. Permeameters with diameter sizes of 3.8, 7, 10 and 14 cm were used in this study. The penetration depth decreased with increasing diameter and then remained constant afterwards.

The stability of sand permeated with bentonite suspensions was studied under increasing hydraulic gradients. Hydraulic conductivity tests were conducted at various hydraulic gradients to determine the critical gradient at which washing out is initiated. The threshold bentonite content is around 3% by weight of bentonite to weight of sand. Below the threshold bentonite content, the flow was occurring through voids in the sand that were not fully permeated with bentonite and hence the hydraulic conductivity was almost equal to that of clean sand. However, permeated sand samples with bentonite content greater than 3% indicated lower hydraulic conductivities initially since the water is forced to flow through the bentonite voids rather than the sand voids.

CHAPTER 5: ANALYSIS

5.1 Introduction

This chapter links the rheological properties of modified and unmodified bentonite suspensions, penetrability of bentonite suspensions into sand, and the stability of sands permeated with bentonite suspensions. The penetration of bentonite suspensions into sand depends on the bentonite and sand physical properties as well as the rheological properties of the bentonite suspensions; equilibrium viscosity. A relation is determined between the yield stress of bentonite suspensions and the critical hydraulic gradient that initiates washing out and the final gradient after which the hydraulic conductivity remains almost constant.

5.2 Penetration depth

Yoon (2011) estimated an empirical equation that predicts the penetration distance of bentonite suspensions into sand based on the apparent viscosity of the grout and the grain sizes of the grout and soil. The empirical equation is as follows:

$$h\,(cm) = \Phi_1 \left[\frac{\left(\frac{P}{1atm}\right)^{\Phi_2}}{\left(\mu_{r,equilibrium}\right)^{\Phi_3}} \left(N_c{}^{\Phi_4}\right) \right] \left[e^{\left(\Phi_5 \frac{FC}{100}\right)} \right] \qquad \text{Equation 15}$$

Where h is the penetration distance (cm), Φ1 is the scaling constant (cm), Φ2 is the empirical constant for normalized pressure (dimensionless), Φ3 is the empirical constant for normalized viscosity (dimensionless), Φ4 is the empirical constant for normalized effective grain size (dimensionless), Φ5 is the empirical constant for fine contents (dimensionless), P is the injection pressure (kPa), $\mu_{r,equilibrium}$ is the relative viscosity at the equilibrium shear rate (μsuspensions (Pa·s)/ μwater (Pa·s)), FC is the non-plastic fines content in granular soils (%),

and Nc is the normalized effective grain size of sand (d_{10},sand (mm) / d_{95} ,bentonite (mm)), where the effective grain size is considered as a property of sand without considering its change due to the presence of fines.

All the parameters were normalized in order to achieve dimensionless numbers. The proposed correlation was calibrated using experimental data using a root mean square error method resulting in the empirical constants of Φ_1, Φ_2, Φ_3 and Φ_4 of 0.79, 0.28, 1.41, and 4.51, respectively (Yoon, 2011). In this study, sand was permeated with bentonite suspensions in permeameters of different diameter sizes. Based on the results, the penetration length of slurry was reduced as the diameter of permeameter increases, but become constant beyond a certain diameter (7.0 cm in this study), implying that the scale effect of the tests was diminished. The latter can be seen in Figure 5-1. Based on this observation, the empirical constant Φ_1 was corrected to 0.32. Figure 5-2 shows the conformance of the experimental results with the penetration length predicted by the adjusted empirical equation for a pressure of 35 kPa.

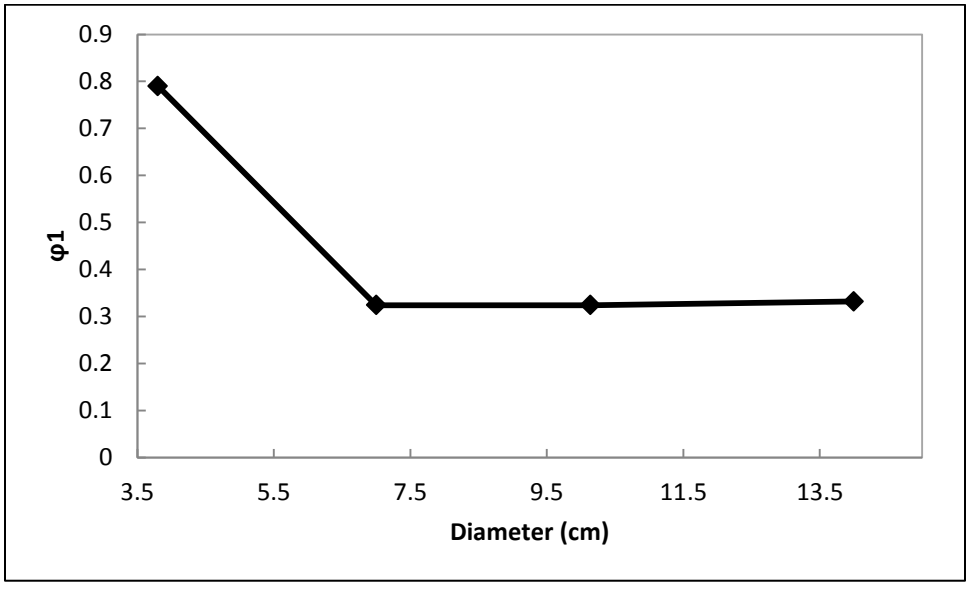

Figure 5-1: Scaling factor versus diameter of permeameter

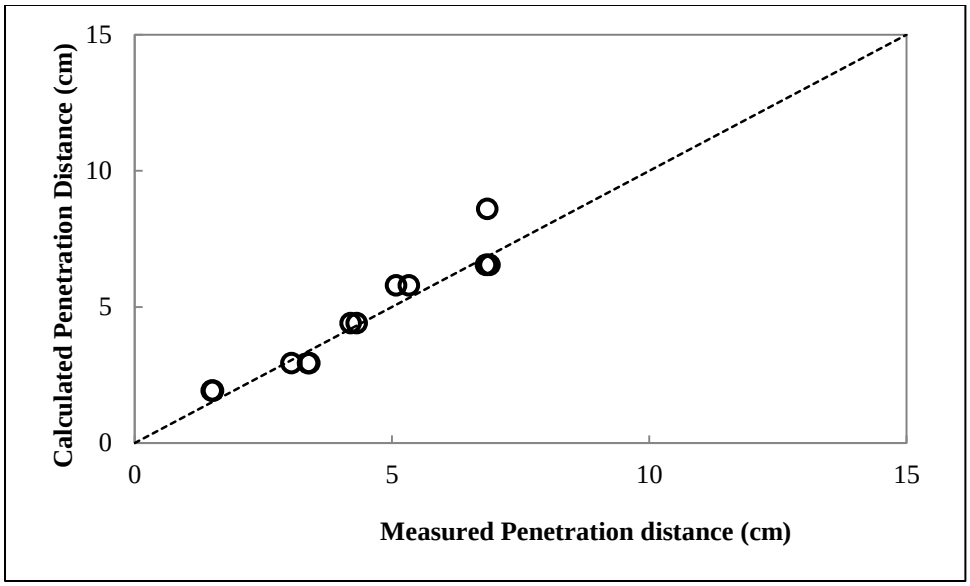

Figure 5-2: Calculated versus measured penetration distance compared to a 45 degrees line

5.3 Stability of sand permeated with bentonite suspensions

The washing out results can be grouped into two categories based on the bentonite content: bentonite content below threshold content and bentonite content above threshold content. Based on the hydraulic conductivity tests performed in this study and by Yoon (2011), the threshold bentonite content is about 3%. Figures 4-23 and 4-24 show 2 examples of specimens with bentonite content less that the critical threshold. In both cases, as the hydraulic gradient increases, the change in measured hydraulic conductivity was minimal. For these specimens, the bentonite suspension is not enough to fill out all the voids within the sand skeleton, and therefore, there will still be some "water channels" that allow for water flow around the bentonite suspension. This is reflected by a higher initial hydraulic conductivity at low gradients as compared to specimens with bentonite contents exceeding the threshold content.

For the specimens with higher bentonite contents, the water flow occurs through the voids within the bentonite suspension (also known as clay void ratio). As a result, the initial measured hydraulic conductivity for these specimens is lower than that recorded for the

specimens with lower bentonite contents. For specimens with bentonite content higher than the threshold content, there was a clear increase in hydraulic conductivity when the hydraulic gradient increases and washing out initiates. This increase in hydraulic conductivity is accompanied with an observed mobilization of the bentonite from the sand. When washing out occurs, the effluent form the sand into the top filter material is no longer a clear water but rather cloudy.

The bentonite content usually decreases after the washing out tests are completed with specimens experiencing a significant increase in hydraulic conductivity showing a larger change in the bentonite contents. Overall, the bentonite content at the top of the specimens was higher than that at the bottom of the specimen after the conclusion of the washing out tests. A residual bentonite content seems to be immobile from the sand once permeated. As a result, the hydraulic conductivity of all specimens at the end of the washing out tests (and throughout most of the decreasing gradient tests) have a similar hydraulic conductivity on the order of 10^{-3}cm/sec. While this high hydraulic conductivity indicate flow though the sand void ratio, its magnitude (about 10 times lower than that of clean sand) indicate that the available void space for water flow has been reduced.

CHAPTER 6: CONCLUSIONS AND FUTURE WORK

6.1 Summary of Conclusions

The rheological properties of unmodified and modified bentonite suspensions were investigated in this study to evaluate the effects of the rheological properties on the penetration depth of bentonite suspensions into sand and their post-grouting stability under increasing hydraulic gradients. The study generated the following conclusions:

1. The yield stress, equilibrium viscosity, loss modulus, and storage modulus increase as the bentonite fraction in the bentonite suspensions increases. Conversely, the critical strain and phase angle decrease as the bentonite fraction increases.
2. The yield stress, equilibrium viscosity, loss modulus, and storage modulus increase over time; whereas, the critical strain and phase angle decrease. The increase or decrease in the rheological parameters is rapid after initial mixing but then it converges.
3. The addition of sodium pyrophosphate (SPP), an additive, to bentonite suspensions significantly reduces yield stress, equilibrium viscosity, loss modulus, and storage modulus. However, the reduced parameters gradually increase with time. After initial mixing, the recovery process is rapid but then it converges and becomes slow.
4. The penetration depth of bentonite suspensions into soils depends on the equilibrium viscosity of bentonite suspensions, the grain size distribution of the bentonite and the soil, and the injection pressure. The stoppage of flow of bentonite suspensions into soil depends on filtration. Yoon's (2011) empirical equation to predict the penetration depth of bentonite suspensions into sand was adjusted to accommodate for large grouting areas similar to field conditions.

5. The hydraulic conductivity of the sand permeated with bentonite suspensions depends on the bentonite content and clay void ratio. Water flows through voids in the sand matrix when the bentonite content is less than 3%, whereas, flow is governed by the clay voids when the bentonite content is greater than 3%. The bentonite content affects the clay void ratio which determines if the skeletal pores are filled and blocked with enough bentonite to force the water flow to be through the clay voids rather than sand voids.
6. The post grouting stability of sand permeated with bentonite suspensions depends on the bentonite content, the bentonite suspensions' yield stress, and external hydraulic gradients. For specimens with bentonite content less than the threshold bentonite content of 3%, minimal washing out was observed. However, the hydraulic conductivity was not reduced significantly because of remaining water flow channels within the sand voids. For sands with higher bentonite content, mobilization of bentonite suspensions occurs as the external hydraulic gradient increases and exceeds the threshold hydraulic gradients. In both cases, after permeating sand with bentonite suspensions, a residual amount of bentonite will be permanently placed within the voids and cannot be removed even with gradients high enough to cause washing out.

6.2 Recommendations for Future Work

This objective of this study is to highlight the possibility of using bentonite suspensions to permeate soils to enhance the hydraulic performance of granular soils. The proposed empirical equation helps in estimating the penetration depth of bentonite suspensions into soil. However, the post grouting stability of these soils permeated with bentonite suspensions is key to ensure the continuity of their performance. The washout tests conducted in this study show that once the

threshold hydraulic gradient is exceeded, bentonite suspensions are mobilized and washing out continues to occur until the gradient is dropped below the threshold.

There is a relation between the yield stress of the bentonite suspensions and the threshold hydraulic conductivity; however, not enough washing out tests are available to determine this relation. It is recommended to relate the threshold hydraulic gradients to Cambfort (1964) stability equation and to relate the yield stress to the stresses developed in the permeated sand which are predicted according to Equation 13.

REFERENCES

Abend, S., and Lagaly, G. (2000). "Sol-gel transitions of sodium Montmorillonite dispersions," Applied Clay Science, Vol. 16, No. 3-4, pp. 201-227.

Abichou, T., Benson, C. H., and Edil, T. B. (2000). "Foundry Green Sands as Hydraulic Barriers: Laboratory Study," Journal of Geotechnical and Geoenvironmental Engineering, Vol. 126, No. 12, pp. 1174-1183.

Akbulut, S., and Saglamer, A. (2002). "Estimating the groutability of granular soils: a new approach," Tunneling and Underground Spaces Technonlogy, Vol. 17, No.4, pp. 371-380.

ASTM D 422-63 (2002). "Standard test method for particle-size analysis of soils," American society for testing and materials, Philadelphia, PA.

ASTM D854-02 (2002). "Standard test methods for specific gravity of soil solids by water pycnometer," American society for testing and materials, Philadelphia, PA.

ASTM D4253-00 (2006). "Standard test methods for maximum index density and unit weight of soils using a vibratory table," American society for testing and materials, Philadelphia, PA.

ASTM D4254-00 (2006). "Standard test methods minimum index density and unit weight of oils and calculation of relative density," American society for testing and materials, Philadelphia, PA.

ASTM D 4318-00 (2000). "Standard test methods for liquid limit, plastic limit, and plasticity index of soils," American society for testing and materials, Philadelphia, PA.

ASTM D5856-95 (2007). "Standard Test Method for Measurement of Hydraulic Conductivity of Porous Material Using a Rigid-Wall, Compaction mold Permeameter," American society for testing and materials, Philadelphia, PA.

Axelsson M., Gustafson, G., and Fransson, Å. (2009). "Stop mechanism for cementitious grouts at different water-to-cement ratios," Tunneling and Underground Space Technology, Vol. 24, pp. 390-397.

Barnes, H.A., and Carnali, J.O. (1990). "The vane-in-cup as a novel rheometer geometry for shear thinning and thixotropic materials," Journal of. Rheology, Vol. 34, pp. 841-867.

Barnes, H.A., and Nguyen, Q.D. (2001). "Rotating vane rheometry a review," Journal of Non Newtonian Fluid Mechanics, Vol. 98, No. 1, pp. 1-14.

Borgesson, L., Johannesson, L., and Gunnarsson, D. (2003). "Influence of soil structure heterogeneities on the behaviour of backfill materials based on mixtures of bentonite and crushed rock," Applied Clay Science, Vol. 23, pp. 121-131.

Brandenburg, U., and Lagaly, G. (1988). "Rheological properties of sodium montmorillonite dispersions," Applied Clay Science Vol.3, pp. 263-279.

Bryant, S., King, P., and Mellor, D. 1993*a*. Network model evaluation of permeability and spatial correlation in a real random sphere packing. Transport in Porous Media, **11**: 53-70.

Bryant, S., Mellor, D., and Cade, C. 1993*b*. Physically representative network models of transport in porous media. AIChE Journal, **39**(3): 387–396.

Burwell E.B. (1958). "Cement, clay grouting of foundations: Practice of the corps of engineering," Journal of the Soil Mechanics and Foundations Division, ASCE, Vol. 84, No. 1551, pp. 1-22.

Cambefort, H. (1964). "Injection des Sols," Eyrolles, Paris.

Callaghan, I.C., and Ottewill, R.H. (1974). "Interparticle forces in montmorillonite gels," Discussion of Faraday Society, Vol. 57, pp. 110-118.

Castelbaum, D., and Shackelford, C. (2009). "Hydraulic conductivity of bentonite slurry mixed sands," Journal of Geotechnical and Geoenvironmental Engineering. Vol. 135, No. 12, pp. 1941-1956.

Chapuis, R. (2002). "The 2000 RM Hardy Lecture: Full-scale hydraulic performance of soil-bentonite and compacted clay liners," Canadian Geotechnical Journal. Vol. 39, No. 2, pp. 417-439.

Clarke, J. P. (2008). "Investigation of time-dependent rheological behavior of sodium pyrophosphate-bentonite suspensions,". M.S. Thesis, Purdue University, West Lafayette, IN.

de Vries G., Koelewijn A.R. and Hopman V. "IJkdijk Full Scale Underseepage Erosion (Piping) Test: Evaluation of Innovative Sensor Technology".

Duran, J.D.G., Ramos-Tejada, M.M., Arroyo, F.J., Gonzalez-Caballero, F. (2000). "Rheology and electrokinetic properties of sodium montmorillonite suspensions," Journal of Colloid and Interface Science, pp. 107-117.

Fukushima, Y. (1984). "X-ray diffraction study of aqueous montmorillonite emulsions," Clay and Clay Minerals, Vol. 32, No.4, pp. 320-326.

Geier, D.L. (2004). "Rheological investigation of bentonite based suspensions for geotechnical

applications," Thesis, Purdue University, West Lafayette, IN.

Goh, R., Leong, Y. K., and Lehane, B. (2011). "Bentonite slurries-zeta potential, yield stress, adsorbed additive and time-dependent behaviour," Rheologica Acta, Vol. 50, pp. 29-38.

Haltz, R.D., and Kovacs, W.D. (1981). "An introduction to geotechnical engineering," Prentice Hall, New Jersey.

Herzig, J.P., Leclerc, D.M., Le Goff, P. (1970). "Flow of suspensions through porous media. Application to deep filtration." Industrial and engineering chemistry Vol. 62, No. 5, pp. 8-35.

Heiser, J.H., and B. Dwyer. (1997). "Summary report on close-coupled subsurface barrier technology initial field trials to full-scale demonstration." Brookhaven National Laboratory, BNL-52531.

Hwang, H. (2010). "The effects of prehydration on hydraulic conductivity of SBMs," M.S. Thesis, The University of Texas at Austin, Austin, TX.

Kasperski, K.L., Helper, ch. T. and Helper, L.G., (1986). "Viscosities of dilute aqueous suspensions of montmorillonite and kaolinite clays," Canadian Journal of Chemistry, Vol. 64, pp. 1919-1924.

Karol, R.H. (2003). "Chemical grouting and soil stabilization," 3rd ed. Marcel Dekker, New York.

Kaoser, S., Barrington, S., Elektorowicz, M., and Ayadat, T. (2006). "The influence of hydraulic gradient and rate of erosion on hydraulic conductivity of sand-bentonite mixtures," Soil and Sediment Contamination, Vol. 15, No. 5, pp. 481-496.

Kenney, T.C., van Veen, W.A., Swallow, M.A., and Sungaila, M.A. (1992). "Hydraulic conductivity of compacted bentonite-sand mixtures" Canadian Geotechnical Journal, Vol. 29, No. 3, pp. 364-374.

Kelessidis, V. C., Tsamantaki, C., and Dalamarinis, P. (2007). "Effect of pH and electrolyte on the rheology of aqueous wyoming bentonite dispersions," Applied Clay Science, Vol. 38, No. 1-2, pp. 86-96.

Kolb C.R. (1976). "Geologic Control of Sand Boils Along Mississippi River Levees," Geomorphology and Engineering, Geomorphology Symposium, Binghamton, NY.

Komine, H., and Ogata, N. (2003), "New equations for swelling characteristics of bentonite-based buffer materials," Canadian Geotechnical Journal Vol. 40, pp. 460-475.

Lagaly, G. (1989). "Principles of flow of kaolin and bentonite dispersions," Applied Clay Science, Vol. 4, pp. 105-123.

Mahaut, F., Chateau, X., Coussot, P., Ovarlez, G. (2008). "Yield stress and elastic modulus of suspensions of noncolloidal particles in yield stress fluids," Journal of Rheology, Vol.52, pp. 287-313.

Metcafle, R., and Walker (2004). "Bentonite-cement interaction in repository environments," Proceedings of the international workshop, 14-16 April 2004, Tokyo, NUMO-TR-04-05, Nuclear Waste Management Organization of Japan, Tokyo, pp 27-29.

Mitchell, J.K. (1993). "Fundamentals of soil behavior," 2nd ed. Wiley, New York.

Mourchid, A., Delville, A., Lambard, J., Lecolier, E., and Levitz, P. (1995). "Phase diagram of colloidal dispersions of anisotropic charged particles: equilibrium properties, structure, and rheology of laponite suspensions," Langmuir, Vol.11, No. 6, pp. 1942-1950.

Nguyen, Q., Akroyd, T., De Kee, D., and Zhu, L. (2006). "Yield stress measurements in suspensions: an inter-laboratory study," Korea-Australia Rheology. Journal. Vol. 18, No.1, pp.15-24.

Nguyen, Q.D., and Boger, D.V. (1985). "Direct yield stress measurement with the vane method," Journal of Rheology, Vol. 29, No. 3, pp. 335-347.

Penner, D., and Lagaly, G. (2001). "Influence of anions on the rheological properties of clay mineral dispersions," Applied. Clay Science Vol. 19, No. 1-6, pp. 131-142.

Pearlman (1999). "Subsurface contaminant and monitoring systems: barriers and beyond," U.S EPA, Washington D.C.

Rugg, D. (2010). "Undrained monotonic shear strength of loose saturated sand treated with thixotropic bentonite suspension for soil improvement," M.S. Thesis, The University of Texas at Austin, Austin, TX.

Saada, Z., Canou, J., Dormieux, L., Dupla, J.C., and Maghous, S. (2005). "Modeling of cement suspension flow in granular porous media," International Journal for Numerical and Analytical Methods in Geomechanics. Vol. 29, pp. 691-711.

Santagata, M., and Santagata, E. (2003). "Experimental investigation of factors affecting the injectability of microcement grouts," Proceedings of the 3rd International Conference, ASCE, Geotechnical special publication 120, pp. 1221-1234.

Santamarina, J., Klein, K.A., Wang, Y.H., Prencke, E. (2002). "Specific surface: determination and relevance," Canandian Geotechnical Journal, Vol. 39, pp. 233-241.

Smyth, D., Cherry, J., and Jowett, R. (1995). "Sealable joint steel sheet piling for groundwater pollution control," Proceedings of ER '95: Committed to Results, U.S. Department of Energy, Denver, CO.

Stern, O. (1924). "Zur Theorie der Elektrolytischen Doppelschriht," Zeitschrift Electrochem, Vol. 30, pp. 508-516.

Stokes, J.R., and Telford, J.H. (2004). "Measuring the yield behaviour of structured fluids," Journal of Non-Newtonian Fluid Mechanics, Vol.124, pp.137-146.

Tombácz, E., and Szerkeres, M. (2004). "Colloidal behavior of aqueous montmorillonite suspensions: the specific role of pH in the presence of indifferent electrolytes," Applied Clay Science, Vol. 27, pp. 75-94.

Turnbull W.J., and Mansur C.I. (1959). "Investigation of Underseepage-Mississippi River Levees," Transactions, ASCE, Vol. 126, No.1, pp. 1429-1485.

Uhlherr, P.H.T., Guo, J, Tiu, C., Zhang, X.M., Zhou, J.Z.Q, and Fang, T.N. (2005). "The shear-induced solid liquid transition in yield stress materials with chemically different structures," Journal of Non-Newtonian Fluid Mechanics, Vol. 125, pp. 101-119.

van Olphen, H. (1977). "An Introduction to Clay Colloid Chemistry," Wiley, New York.

Wolff T.F. (1987). "Levee Underseepage Analysis for Special Foundation Conditions," Research report prepared for USACE Waterways Experiment Station, Michigan State University, East Lansing, MI.

Yoon, Jisuk and El Mohtar, Chadi, "Disturbance Effect on Time-Dependent Yield Stress Measurement of Bentonite Suspensions," Geotechnical Testing Journal, Vol. 36, No. 1, 2013, pp. 1–10, doi:10.1520/GTJ20120082. ISSN 0149-6115.

Yoon J. and El Mohtar C. (2013). "Groutablity of granular soils using sodium pyrophosphate modified bentonite suspensions," Tunnelling and Underground Space Technology Journal, Vol 37, 2013, pp. 135-145.

Yoon, J. (2011). "Application of pore fluid engineering for improving the hydraulic performance of granular soils," PhD Dissertation, The University of Texas at Austin, Austin, TX.

Zhu, L., Sun, N., Papadopoulos, K., and de Kee, D. (2001). "A slotted plate device for measuring static yield stress," Journal of Rheology Vol. 45, pp.1105-1123.